
A Mean Field Theory of Quantized Deep Networks: The Quantization-Depth Trade-Off

Yaniv Blumenfeld
Technion, Israel
yanivblm6@gmail.com

Dar Gilboa
Columbia University
dargilboa@gmail.com

Daniel Soudry
Technion, Israel
daniel.soudry@gmail.com

Abstract

Reducing the precision of weights and activation functions in neural network training, with minimal impact on performance, is essential for the deployment of these models in resource-constrained environments. We apply mean field techniques to networks with quantized activations in order to evaluate the degree to which quantization degrades signal propagation at initialization. We derive initialization schemes which maximize signal propagation in such networks, and suggest why this is helpful for generalization. Building on these results, we obtain a closed form implicit equation for L_{\max} , the maximal trainable depth (and hence model capacity), given N , the number of quantization levels in the activation function. Solving this equation numerically, we obtain asymptotically: $L_{\max} \propto N^{1.82}$.

1 Introduction

As neural networks are increasingly trained and deployed on-device in settings with memory and space constraints [12, 5], a better understanding of the trade-offs involved in the choice of architecture and training procedure are gaining in importance. One widely used method to conserve resources is the quantization (discretization) of the weights and/or activation functions during training [6, 24, 13, 3]. When choosing a quantized architecture, it is natural to expect depth to increase the flexibility of the model class, yet choosing a deeper architecture can make the training process more difficult. Additionally, due to resource constraints, when using a quantized activation function whose image is a finite set of size N , one would like to choose the smallest possible N such that the model is trainable and performance is minimally affected. There is a trade-off here between the capacity of the network which depends on its depth and the ability to train it efficiently on the one hand — and the parsimony of the activation function used on the other.

We quantify this trade-off between capacity/trainability and the degree of quantization by an analysis of wide neural networks at initialization. This is achieved by studying *signal propagation* in deep quantized networks, using techniques introduced in [23, 25] that have been applied to numerous architectures. Signal propagation will refer to the propagation of correlations between inputs into the hidden states of a deep network. Additionally, we consider the dynamics of training in this regime and the effect of signal propagation on the change in generalization error during training.

In this paper,

- We suggest (section 3.2) that if the signal propagation conditions do not hold, generalization error in early stages of training should not decrease at a typical test point, potentially explaining the empirically observed benefit of signal propagation to generalization. This is done using an analysis of learning dynamics in wide neural networks, and corroborated numerically.
- We obtain (section 4.2) initialization schemes that maximize signal propagation in certain classes of feed-forward networks with quantized activations.

- Combining these results, we obtain an expression for the trade-off between the quantization level and the maximal trainable depth of the network (eq. 18), in terms of the depth scale of signal propagation. We experimentally corroborate these predictions (Figure 3).

2 Related work

Several works have shown that training a 16 bit numerical precision is sufficient for most machine learning applications [10, 7], with little to no cost to model accuracy. Since, many more aggressive quantization schemes were suggested [13, 17, 21, 20], ranging from the extreme usage of 1-bit at representations and math operations [24, 6], to a more conservative usage of 8-bits [3, 27], all in effort to minimize the computational cost with minimal loss to model accuracy. Theoretically, it is well known that a small amount of imprecision can significantly degrade the representational capacity of a model. For example, an infinite precision recurrent neural network can simulate a universal Turing machine [26]. However, any numerical imprecision reduces the representational power of these models to that of finite automata [18]. In this paper, we focus on the effects of quantization on training. So far, these effects are typically quantified empirically, though some theoretical work has been done in this direction (e.g. [16, 1, 33, 31]).

Signal propagation in wide neural networks has been the subject of recent work for fully-connected [23, 25, 22, 30], convolutional [29] and recurrent architectures [4, 8]. These works study the evolution of covariances between the hidden states of the network and the stability of the gradients. These depend only on the leading moments of the weight distributions and the nonlinearities at the infinite width limit, greatly simplifying analysis. They identify critical initialization schemes that allow training of very deep networks (or recurrent networks on long time sequence tasks) without performing costly hyperparameter searches. While the analytical results in these works assume that the layer widths are taken to infinity sequentially (which we will refer to this as the *sequential* limit), the predictions prove predictive when applied to networks with layers of equal width once the width is typically of the order of hundreds of neurons. For fully connected networks it was also shown using an application of the Central Limit Theorem for exchangeable random variables that the asymptotic behavior at infinite width is independent of the order of limits [19].

3 Preliminaries: the mean field approach

3.1 Signal propagation in feed-forward networks

We now review the analysis of signal propagation in feed-forward networks performed in [23, 25]. The network function $f : \mathbb{R}^{n_0} \rightarrow \mathbb{R}^{n_{L+1}}$ is given by

$$\begin{aligned} \phi(\alpha^{(0)}(x)) &= x \\ \alpha^{(l)}(x) &= W^{(l)}\phi(\alpha^{(l-1)}(x)) + b^{(l)} \quad l = 1, \dots, L \\ f(x) &= \alpha^{(L+1)}(x) \end{aligned} \tag{1}$$

for input $x \in \mathbb{R}^{n_0}$, weight matrices $W^{(l)} \in \mathbb{R}^{n_l \times n_{l-1}}$ and nonlinearity $\phi : \mathbb{R} \rightarrow \mathbb{R}$. The weights are initialized using $W_{ij}^{(l)} \sim \mathcal{N}(0, \frac{\sigma_w^2}{n^{(l-1)}})$, $b_i^{(l)} \sim \mathcal{N}(0, \sigma_b^2)$ so that the variance of the neurons at every layer is independent of the layer widths ¹.

According to Theorem 4 in [19], under a mild condition on the activation function that is satisfied by any saturating nonlinearity, the *pre-activations* $\alpha^{(l)}(x)$ converge in distribution to a multivariate Gaussian as the layer widths n_1, \dots, n_L are taken to infinity in any order (with n_0, n_{L+1} finite) ². In the physics literature the approximation obtained by taking this limit is known as the *mean field approximation*.

¹In principle the following results should hold under more generally under mild moment conditions alone.

²When taking the sequential limit, asymptotic normality is a consequence of repeated application of the Central Limit Theorem [23]

The covariance of this Gaussian at a given layer is then obtained by the recursive formula

$$\begin{aligned}\mathbb{E}\alpha_i^{(l)}(x)\alpha_j^{(l)}(x') &= \mathbb{E} \sum_{k,k'=1}^{n_l-1} W_{ik}^{(l)} W_{jk'}^{(l)} \phi(\alpha_k^{(l-1)}(x))\phi(\alpha_{k'}^{(l-1)}(x')) + b_i^{(l)}b_j^{(l)} \\ &= \left[\sigma_w^2 \mathbb{E}\phi(\alpha_1^{(l-1)}(x))\phi(\alpha_1^{(l-1)}(x')) + \sigma_b^2 \right] \delta_{ij}.\end{aligned}\quad (2)$$

Omitting the dependence on the inputs x, x' in the RHS below, we define

$$\begin{pmatrix} \mathbb{E}\alpha_i^{(l)}(x)\alpha_i^{(l)}(x) & \mathbb{E}\alpha_i^{(l)}(x)\alpha_i^{(l)}(x') \\ \mathbb{E}\alpha_i^{(l)}(x)\alpha_i^{(l)}(x') & \mathbb{E}\alpha_i^{(l)}(x')\alpha_i^{(l)}(x') \end{pmatrix} = Q^{(l)} \begin{pmatrix} 1 & C^{(l)} \\ C^{(l)} & 1 \end{pmatrix} = \Sigma(Q^{(l)}, C^{(l)}). \quad (3)$$

Combining eqs. 2 and 3 we obtain the following two-dimensional dynamical system:

$$\begin{pmatrix} Q^{(l)} \\ C^{(l)} \end{pmatrix} = \begin{pmatrix} \sigma_w^2 \mathbb{E}_{u \sim \mathcal{N}(0, Q^{(l-1)})} \phi^2(u) + \sigma_b^2 \\ \frac{1}{Q^{(l-1)}} \left[\sigma_w^2 \mathbb{E}_{(u_1, u_2) \sim \mathcal{N}(0, \Sigma(Q^{(l-1)}, C^{(l-1)})} \phi(u_1)\phi(u_2) + \sigma_b^2 \right] \end{pmatrix} \equiv \mathcal{M} \left[\begin{pmatrix} Q^{(l-1)} \\ C^{(l-1)} \end{pmatrix} \right], \quad (4)$$

where \mathcal{M} depends on the nonlinearity and the initialization hyperparameters σ_w^2, σ_b^2 and the initial conditions $(Q^{(0)}, C^{(0)})^T$ depend also on x, x' . See Figure 1 for a visualization of the covariance propagation.

Once the above dynamical system converges to a fixed point (Q^*, C^*) or at least approaches it to within numerical precision, information about the initial conditions is lost. As argued in [25], this is detrimental to learning as inputs in different classes can no longer be distinguished in terms of the network output (assuming the fixed point C^* is independent of $C^{(0)}$, see Lemma 1). The convergence rate to the fixed point can be obtained by linearizing the dynamics around it. This can be done for the two dimensional system as a whole, yet in [25] it was also shown that, for any monotonically increasing nonlinearity, convergence of this linearized dynamical system in the direction $C^{(l)}$ cannot be faster than convergence in the $Q^{(l)}$ direction, and thus studying convergence can be reduced to the simpler one dimensional system $C^{(l)} = \mathcal{M}_{Q^*}(C^{(l-1)})$ that is obtained by assuming $Q^{(l)}$ has already converged. The convergence rate is given by the following known results of [25, 8] which we recapitulate for completeness:

Lemma 1. [25, 8] Defining $\Sigma(Q, C) = Q \begin{pmatrix} 1 & C \\ C & 1 \end{pmatrix}$ for $Q \geq 0, C \in [-1, 1]$ the dynamical system

$$\mathcal{M}_{Q^*}(C) = \frac{1}{Q^*} \left[\sigma_w^2 \mathbb{E}_{(u_1, u_2) \sim \mathcal{N}(0, \Sigma(Q^*, C))} \phi(u_1)\phi(u_2) + \sigma_b^2 \right] \quad (5)$$

when linearized around a fixed point C^* , converges at a rate

$$\chi = \left. \frac{\partial \mathcal{M}_{Q^*}(C)}{\partial C} \right|_{C^*} = \sigma_w^2 \mathbb{E}_{(u_a, u_b) \sim \mathcal{N}(0, \Sigma(Q^*, C^*))} \phi'(u_1)\phi'(u_2). \quad (6)$$

Additionally, $\mathcal{M}_{Q^*}(C)$ has at most one stable fixed point in the range $[0, 1]$ for any choice of ϕ such that ϕ is odd or ϕ'' is non-negative.

Proof: See Appendix A.

We subsequently drop the subscript in $\mathcal{M}_{Q^*}(C)$ to lighten notation. The corresponding time scale of convergence in the linearized regime is

$$\xi = -\frac{1}{\log \chi}. \quad (7)$$

χ depends on the initialization hyperparameters and choice of nonlinearity, and it follows from the considerations above that signal propagation from the inputs to the outputs of a deep network would be facilitated by a choice of χ such that ξ diverges, which occurs as χ approaches 1 from below. Indeed, as observed empirically across multiple architectures and tasks [29, 4, 8, 30], up to a constant factor ξ typically gives the maximal depth up to which a network is trainable. These calculations motivate initialization schemes that satisfy:

$$\chi = 1$$

in order to train very deep networks. We will show shortly that this condition is unattainable for a large class of quantized activation functions.³

The analysis of forward signal propagation in the sense described above in networks with continuous activations is related to the stability of the gradients as well [25]. The connection is obtained by relating the rate of convergence χ to the first moment of the state-to-state Jacobian

$$J = \lim_{l \rightarrow \infty} \frac{\partial \hat{\alpha}^{(l)}}{\partial \hat{\alpha}^{(l-1)}}. \quad (8)$$

Taking all the layer widths to be equal to n , the first moment is given by

$$m_{JJ^T} = \frac{1}{n} \mathbb{E} \text{tr} (JJ^T). \quad (9)$$

Since high powers of this matrix will appear in the gradient, controlling its spectrum can prevent the gradient from exploding or vanishing. In the case of quantized activations however, the relationship between the Jacobian and the convergence rate χ no longer holds since the gradients vanish almost surely and modified weight update schemes such as the Straight-Through Estimator (STE) [11, 13] are used instead. However, one can define a modified Jacobian J_{STE} that takes the modified update scheme into account and control its moments instead.

3.2 Signal propagation may improve generalization

The argument that a network will be untrainable if signals cannot propagate from the inputs to the loss, corresponding to rapid convergence of the dynamical system eq. 4, has empirical support across numerous architectures. A choice of initialization hyperparameters that facilitates signal propagation has also been shown to lead to slight improvements in generalization error, yet understanding of this was beyond the scope of the existing analysis. Indeed, there is also empirical evidence that when training very deep networks it is only the generalization error that is impacted adversely but the training error is not [29]. Additionally, one may wonder whether a deep network could still be trainable despite a lack of signal propagation. On the one hand, rapid convergence of the correlation map between the pre-activations is equivalent to the distance between $f(x), f(x')$ converging to a value that is independent of the distance between x, x' . On the other, since deep networks can fit random inputs and labels [32] this convergence may not be an impediment to training.

To understand the effect of signal propagation on generalization, we consider the dynamics of learning for wide, deep neural networks in the setting studied in [14, 15]. We note that this setting introduces an unconventional scaling of the weights. Despite this, it should be a good approximation for the early stages of learning in networks with standard initialization, as long as the weights do not change too much from their initial values. In this regime, the function implemented by the network evolves linearly in time, with the dynamics determined by the Neural Tangent Kernel (NTK). We argue that rapid convergence of eq. 4 in deep networks implies that the error at a typical test point should not decrease during training since the resulting form of the NTK will be independent of the label of the test point. Conversely, this effect will be mitigated with a choice of hyperparameters that maximizes signal propagation, which could explain the beneficial effect on generalization error that is observed empirically. We provide details and empirical evidence in support of this claim for networks with both quantized and continuous activation functions in Appendix L.

4 Mean field theory of signal propagation with quantized activations

In this section, we will explore the effects of using a quantized activation functions on signal propagation in feed-forward networks. We will start by developing the mean field equations for a sign activations and then consider more general activation function, and establish a theory that predicts the relation between the number of quantization states, the initialization parameters and the feed-forward network depth. We conclude by testing the theory predictions on networks' trainability using a standard classification task.

³It will at times be convenient to consider the dynamics of the correlations of the *post-activations* $\hat{\alpha}^{(l)} = \phi(\alpha^{(l)})$ which we denote by $\tilde{\mathcal{M}}(\hat{C})$. The rates of convergence are identical in both cases, as shown in Appendix B.

4.1 Warm-up: sign activations

We begin by considering signal propagation in the network in eq. 1 with $\phi(x) = \text{sign}(x)$. Substituting $\phi(x) = \text{sign}(x)$, $\phi'(u) = 2\delta(u)$ in eqs. 4 and 6 gives

$$Q^* = \sigma_w^2 + \sigma_b^2, \quad \chi = 4\sigma_w^2 \mathbb{E}_{(u_1, u_2) \sim \mathcal{N}(0, \Sigma(Q^*, C^*))} \delta(u_1)\delta(u_2). \quad (10)$$

As shown in Appendix C, we obtain

$$\chi = \frac{2\sigma_w^2}{\pi(\sigma_w^2 + \sigma_b^2)\sqrt{1 - (C^*)^2}} \quad (11)$$

$$\mathcal{M}(C) = \frac{\frac{2\sigma_w^2}{\pi} \arcsin(C) + \sigma_b^2}{\sigma_w^2 + \sigma_b^2}. \quad (12)$$

The closed form expressions 11 and 12, which are not available for more complex architectures, expose the main challenge to signal propagation. It is clear from these expressions that the derivative of $\mathcal{M}(C)$ diverges at 1, and since $\mathcal{M}(C)$ is differentiable and convex, it can have no stable fixed point in $[0, 1]$ that satisfies the signal propagation condition $\chi = 1$. In fact, as we show in Appendix K.1 that the maximal value of χ for this architecture is achievable when $\sigma_b = 0$, and is bounded from above by $\chi_{\max} = \frac{2}{\pi}$ for all choices of the initialization hyperparameters. The corresponding depth scale is bounded by $\xi_{\max} < 3$.

Additionally, one may wonder if using stochastic binary activations [13] might improve signal propagation. In Appendix D we show this is not the case: we consider a stochastic rounding quantization scheme and show that stochastic rounding can only further decrease the signal propagation depth scale.

4.2 General quantized activations

We consider a general activation function $\phi_N : \mathbb{R} \rightarrow S$, where S is a finite set of real numbers of size $|S| = N$. To obtain a flexible class of non-decreasing functions of this form, we define

$$\phi_N(x) = A + \sum_{i=1}^{N-1} H(x - g_i) h_i, \quad (13)$$

where $A \in \mathbb{R}$, $\forall i \in \{1, 2, \dots, N-1\}$, $g_i \in \mathbb{R}$, $h_i \in \mathbb{R}_{>0}$, and $H : \mathbb{R} \rightarrow \mathbb{R}$ is the Heaviside function. This activation function can be thought of as a "stairs" function, going from the minimum state of A to the maximum state $A + \sum_{i=1}^{N-1} h_i$, over $N-1$ stairs, with stair i located at an offset g_i with a height h_i . We will assume that the offsets g_i are ordered, for simplicity. The development of the mean field equations for this activation function is located in appendix E, where we find that:

$$\widehat{Q}^{(l)} = \sum_{i=1}^{N-1} \sum_{j=1}^{N-1} h_i h_j \Psi\left(-\frac{\max(g_i, g_j)}{\sqrt{Q^{(l)}}}\right) \Psi\left(\frac{\min(g_i, g_j)}{\sqrt{Q^{(l)}}}\right), \quad Q^{(l+1)} = \sigma_w^2 \widehat{Q}^{(l)} + \sigma_b^2 \quad (14)$$

$$\chi = \frac{2\sigma_w^2}{\pi Q^* \sqrt{1 - (C^*)^2}} \sum_{i=1}^{N-1} \sum_{j=1}^{N-1} h_i h_j \exp\left[-\frac{g_i^2 - 2C^* g_i g_j + g_j^2}{2Q^* (1 - (C^*)^2)}\right], \quad (15)$$

where $\widehat{Q}^{(l)}$ is the hidden state covariance, as explained in appendix B. This expression diverges as $C^* \rightarrow 1$ since all the summands are non-negative and the diagonal ones simplify to $\frac{2\sigma_w^2 h_i^2}{\pi Q^* \sqrt{1 - (C^*)^2}} \exp\left[-\frac{g_i^2}{2Q^* (1 + C^*)}\right]$. Since $\mathcal{M}(C)$ is convex (see Lemma 1), we find that as in the case of sign activation, $\chi = 1$ is not achievable for any choice of a quantized activation function.

To optimize the signal propagation for any given number of states, we would like to find the parameters that will bring the fixed point slope χ as close as possible to 1. For simplicity, we will henceforth use the initialization $\sigma_b = 0$, which is quite common [9]. Empirical evidence in appendix F suggest that using $\sigma_b > 0$ is sub-optimal, which is not very surprising, given our similar (exact) results for sign activation. For $\sigma_b = 0$, $C = 0$ becomes a fixed point. We eliminate eq. 15 direct dependency on Q^* , by defining *normalized offsets* $\tilde{g} \equiv \frac{g}{\sqrt{Q^*}}$. By moving to normalized offsets,

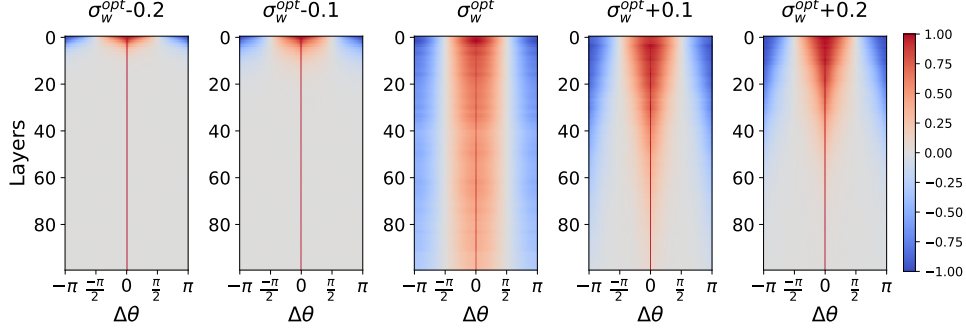


Figure 1: Propagation of empirical covariance between hidden states at different layers, in quantized feed-forward networks with $N = 16$, varying the standard deviation of the weights σ_w . $\Delta\theta$ is the angle between two normalized inputs. Signal propagation is maximized when $\sigma_w = \sigma_w^{\text{opt}}$, and degrades as σ_w deviates from it.

substituting $C^* = 0$ and the remaining Q^* by eq. 14, our expression for the fixed point slope becomes:

$$\chi = \frac{\sum_{i=1}^{N-1} \sum_{j=1}^{N-1} \frac{1}{2\pi} \exp\left[-\frac{1}{2}(\tilde{g}_i^2 + \tilde{g}_j^2)\right] h_i h_j}{\sum_{i=1}^{N-1} \sum_{j=1}^{N-1} \Psi(-\max(\tilde{g}_i, \tilde{g}_j)) \Psi(\min(\tilde{g}_i, \tilde{g}_j)) h_i h_j} \quad (16)$$

Eq. 16 provides us with way to determine the quality of any quantized activation function in regard to signal propagation, without concerning ourselves with the initialization parameters, that will only have a linear effect on the offsets. Since the normalized offsets are sufficient to determine \tilde{Q} , Q , using eq. 15, moving from normalized offsets to actual offsets becomes trivial.

To measure the relation between the number of states and depth scale, we will use equation 16 over a limited set of constant-spaced activations, where we choose $A < 0, \forall i \in \{1, \dots, N-1\}, h_i = \text{const.}$ and the offsets are evenly spaced and centered around zero, with D defined as the distance between two sequential offsets so that $g_i = D(i - \frac{N}{2})$, and \tilde{D} defined as $\tilde{D} = \frac{D}{\sqrt{Q^*}}$. We view this configuration as the most obvious selection of activation function, where the 'stairs' are evenly spaced between the minimal and the maximal state. Using eq. 16 on an activation in this set, we get:

$$\chi = \frac{\sum_{i \in K} \sum_{j \in K} \frac{1}{2\pi} \exp\left[-\frac{1}{2}(i^2 + j^2) \tilde{D}^2\right]}{\sum_{i \in K} \sum_{j \in K} \Psi(-\max(i, j) \tilde{D}) \Psi(\min(i, j) \tilde{D})} \quad (17)$$

when $K = \{k - \frac{N}{2} | \forall k \in \mathbb{N}, k < N\}$. A numeric analysis using of eq. 17 is presented in figure 2, and reveals a clear logarithmic relation between the level of quantization to the optimal fixed point slope, and the normalized spacing required to reach this optimal configuration. By extrapolating the numeric results, as seen in the right panels of 2, We find a good approximations for the the maximal achievable slope for any quantization level $\chi_{\max}(N)$ and the corresponding normalized spacing $D_{\text{opt}}(N)$. Using those extrapolated values, we predict the depth-scale of a quantized, feed-forward network to be:

$$\xi_N = -\frac{1}{\log(\chi_{\max}(N))} \simeq -\frac{1}{\log(1 - e^{0.71} (N+1)^{-1.82})} \simeq \frac{1}{2} (N+1)^{1.82}. \quad (18)$$

where the latter approximation is valid for large N . While the depth scale in eq. 18 is applicable to uniformly spaced quantized activations, numerical results presented in Appendix G suggest that using more complex activations with the same quantization level will not produce better results.

5 Experimental results

To visualize the covariance propagation in eq. 2 we reconstruct an experiment presented in [23], and apply it to untrained quantized neural networks. We consider a neural network with $L = 100$ fully-connected layers, all of width $n = 1000$. We draw two orthonormal vectors $u^0, u^1 \in \mathbb{R}^{1000}$ and generate the 1 dimensional manifold $U = \{u_i = \sqrt{Q_s^*} (u^0 \cos(\theta) + u^1 \sin(\theta)) | i \in \{0, \frac{1}{r}, \frac{2}{r}, \dots, \frac{r-1}{r}\}, \theta = 2\pi i\}$, where $r = 500$ is the num-

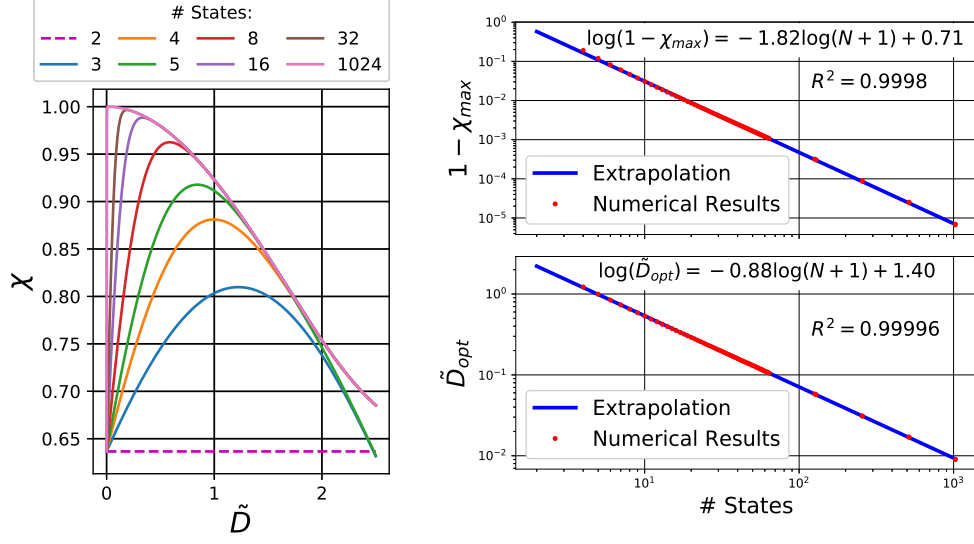


Figure 2: Numerical analysis of the covariance propagation fixed point slope for quantized activation functions. *Left:* The convergence rate in eq. 17 of the covariances of the hidden states as a function of the normalized spacing between offsets \tilde{D} for activations with different levels of quantization N . *Top Right:* The difference between 1 and maximal achievable convergence rate χ_{\max} as a function of N . *Bottom Right:* The normalized spacing between states \tilde{D} corresponding to χ_{\max} as a function of N . We find that the dependence of $1 - \chi_{\max}$ on N is approximated well by a power law.

ber of samples, and Q_s^* is the fixed point, calculated numerically. After initializing the neural network, we use the manifold values as inputs to the neural network and measure the covariance in all hidden layers. We then plot the empirical covariance of the hidden states as a function of the difference in the angle θ of their corresponding inputs. The reason for multiplying the initial values by $\sqrt{Q_s^*}$ is so we can isolate the convergence of the off-diagonal correlations from that of the diagonal.

To test the predictions of the theory, we have constructed a similar experiment to the one described in [25], training neural networks of varying depths over the MNIST dataset. We study how the maximal trainable depth of a quantized activation fully-connected network depends on the weight variance σ_w^2 and the number of states in the activation function N . For our quantized activations, we used the constant-spaced activations we have analyzed in section 4.2:

$$\phi_N(x) = -1 + \sum_{i=1}^{N-1} \frac{2}{N-1} H\left(x - \frac{2}{N-1} \left(i - \frac{N}{2}\right)\right),$$

which describes an activation function with a distance of $D = \frac{2}{N-1}$ between offsets, and with states ranging between -1 and 1.

To find the best initialization parameters for each activation function, we first used eq. 14 to compute \hat{Q}^* assuming our normalized spacing $\frac{D}{\sqrt{Q_s^*}}$ is optimized (\tilde{D}_{opt} , computed using the linear regression parameters of figure’s 2 bottom right panel). Then, we picked $\sigma_b = 0$, $\sigma_w = \frac{1}{\sqrt{Q_s^*}} \frac{D}{\tilde{D}_{\text{opt}}}$, and thus ensured that the normalized offsets are indeed optimal. Gradients are computed using the Straight-Through Estimator (STE) [13]:

$$\Delta_{\text{input}} = \begin{cases} \rho \Delta_{\text{output}} & |\text{input}| < 1 \\ 0 & \text{else} \end{cases} \quad (19)$$

where Δ_{output} is gradient we get from the next layer and Δ_{input} is the gradient we pass to the preceding layer. We pick $\rho^{-1} = \sigma_w \sqrt{\text{erf}\left(\frac{1}{\sqrt{2Q_s^*}}\right)}$ to satisfy the condition of allowing the gradients information to propagate backward, as explained in appendix J. When studying the effect of initialization on trainability of quantized deep networks, (left panel of figure 3), we repeated the same process exactly, but ultimately initialized the weights using the value of σ_w specified on the x-axis. In Appendix H, we add more results that isolate the forward-pass from the backward pass and elaborates on the

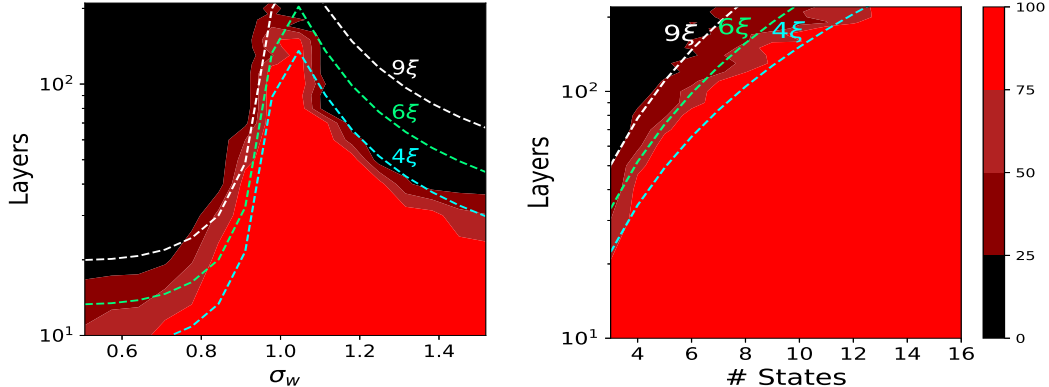


Figure 3: Test accuracy of feed-forward networks of different depth with quantized activation functions trained on MNIST classification after 1600 training steps, compared with the theoretical depth scale predictions (eq. 7). Up to a constant factor, the theoretical depth scale predicts the phase transition between regimes where a network is trainable and one where training fails. *Left*: Networks with a 10 states activation function and different values of the weight variance. *Right*: Networks with different quantization levels (number of states), with variances adjusted to allow optimal signal propagation.

evolution of the training and test accuracy in training time. We also include a simplified initialization scheme in appendix I.

We set the hidden layer width to 2048. We use SGD for training, a learning rate of 10^{-3} for networks with 10-90 layers, and a learning rate of 5×10^{-4} when training 100-220 layers. Those parameters were selected to match those reported in [25], with the second learning rate adjusted to fit our area-of-search. We also use a batch size of 32, and use a standard preprocessing of the MNIST input⁴.

Figure 3 show that initialization of the network using the parameters suggested by our theory achieves the optimal trainability when the number of layers is high. When measuring test accuracy at early stage of the network, we can see that the accuracy is high when the network has $\sim 4\xi$ layers or less. As demonstrated by the advanced training stage results shown in appendix H, and by the results of [25], networks of depth exceeding $\sim 6\xi$ appear to be untrainable.

6 Discussion

In this paper, we study the effect of using quantized activations on the propagation of signals in deep neural networks, from the inputs to the outputs. We focus on quantized activations, which maps its input to a finite set of N possible outputs. Our analysis suggests an initialization scheme that improve network trainability, and that fully-connected networks to become untrainable when the number of layers exceeds $L_{\max} \sim 3(N+1)^{1.82}$.

Additionally, we propose a possible explanation for the improved generalization observed when training networks that are initialized to enable stable signal propagation. While the motivation for the critical initialization has been improved trainability [25], empirically these initialization schemes were shown to improve generalization as well, an observation that was beyond the scope of the analysis which motivated them. By considering the dynamics of learning in wide networks that exhibit poor signal propagation, we find that generalization error in early stages of training will typically not improve. This effect will be minimized when using a critical initialization.

The limitations of poor signal propagation can perhaps be overcome with certain modifications to the architecture or training procedure. One such modification is batch normalization, which we did not consider in the analysis. Some studies [3, 6, 13] have already suggested that applying proper batch normalization is key when training quantized feed-forward networks. There are, however, cases where batch normalization does not work well, like in the case of recurrent neural networks. We expect our findings to have as increased significance if generalized to such architectures, as was done previously for continuous activations [4, 8].

⁴The code for running this experiment and more is provided in https://github.com/yanivb16/quantized_meanfield.

Acknowledgements

The work of DS was supported by the Israel Science foundation (grant No. 31/1031), the Taub Foundation and by a Titan Xp donated by the NVIDIA Corporation. The work of DG was supported by the NSF NeuroNex Award DBI-1707398 and the Gatsby Charitable Foundation.

References

- [1] Alexander G. Anderson and Cory P. Berg. The High-Dimensional Geometry of Binary Neural Networks. *ICLR*, (2014):1–13, 2018.
- [2] Sanjeev Arora, Simon S Du, Wei Hu, Zhiyuan Li, Ruslan Salakhutdinov, and Ruosong Wang. On exact computation with an infinitely wide neural net. *arXiv preprint arXiv:1904.11955*, 2019.
- [3] Ron Banner, Itay Hubara, Elad Hoffer, and Daniel Soudry. Scalable methods for 8-bit training of neural networks. In *Advances in Neural Information Processing Systems*, pages 5145–5153, 2018.
- [4] Minmin Chen, Jeffrey Pennington, and Samuel S Schoenholz. Dynamical isometry and a mean field theory of rnns: Gating enables signal propagation in recurrent neural networks. *arXiv preprint arXiv:1806.05394*, 2018.
- [5] Wenlin Chen, James Wilson, Stephen Tyree, Kilian Weinberger, and Yixin Chen. Compressing neural networks with the hashing trick. In *International Conference on Machine Learning*, pages 2285–2294, 2015.
- [6] Matthieu Courbariaux, Itay Hubara, Daniel Soudry, Ran El-Yaniv, and Yoshua Bengio. Binarized neural networks. *Advances in Neural Information Processing Systems*, 2016.
- [7] Dipankar Das, Naveen Mellempudi, Dheevatsa Mudigere, Dhiraj Kalamkar, Sasikanth Avancha, Kunal Banerjee, Srinivas Sridharan, Karthik Vaidyanathan, Bharat Kaul, Evangelos Georganas, et al. Mixed precision training of convolutional neural networks using integer operations. *arXiv preprint arXiv:1802.00930*, 2018.
- [8] Dar Gilboa, Bo Chang, Minmin Chen, Greg Yang, Samuel S Schoenholz, Ed H Chi, and Jeffrey Pennington. Dynamical isometry and a mean field theory of lstms and grus. *arXiv preprint arXiv:1901.08987*, 2019.
- [9] Xavier Glorot and Yoshua Bengio. Understanding the difficulty of training deep feedforward neural networks. In *Proceedings of the thirteenth international conference on artificial intelligence and statistics*, pages 249–256, 2010.
- [10] Suyog Gupta, Ankur Agrawal, Kailash Gopalakrishnan, and Pritish Narayanan. Deep learning with limited numerical precision. In *International Conference on Machine Learning*, pages 1737–1746, 2015.
- [11] G Hinton. Neural networks for machine learning. coursera,[video lectures], 2012.
- [12] Andrew G Howard, Menglong Zhu, Bo Chen, Dmitry Kalenichenko, Weijun Wang, Tobias Weyand, Marco Andreetto, and Hartwig Adam. Mobilenets: Efficient convolutional neural networks for mobile vision applications. *arXiv preprint arXiv:1704.04861*, 2017.
- [13] Itay Hubara, Matthieu Courbariaux, Daniel Soudry, Ran El-Yaniv, and Yoshua Bengio. Quantized neural networks: Training neural networks with low precision weights and activations. *The Journal of Machine Learning Research*, 18(1):6869–6898, 2017.
- [14] Arthur Jacot, Franck Gabriel, and Clément Hongler. Neural tangent kernel: Convergence and generalization in neural networks. June 2018.
- [15] Jaehoon Lee, Lechao Xiao, Samuel S Schoenholz, Yasaman Bahri, Jascha Sohl-Dickstein, and Jeffrey Pennington. Wide neural networks of any depth evolve as linear models under gradient descent. *arXiv preprint arXiv:1902.06720*, 2019.
- [16] Hao Li, Soham De, Zheng Xu, Christoph Studer, Hanan Samet, and Tom Goldstein. Training Quantized Nets: A Deeper Understanding. *NIPS*, jun 2017.
- [17] Xiaofan Lin, Cong Zhao, and Wei Pan. Towards accurate binary convolutional neural network. In *Advances in Neural Information Processing Systems*, pages 345–353, 2017.

- [18] Wolfgang Maass and Pekka Orponen. On the Effect of Analog Noise in Discrete-Time Analog Computations. *Neural Computation*, 10(5):1071–1095, jul 1998.
- [19] Alexander G de G Matthews, Mark Rowland, Jiri Hron, Richard E Turner, and Zoubin Ghahramani. Gaussian process behaviour in wide deep neural networks. *arXiv preprint arXiv:1804.11271*, 2018.
- [20] Asit Mishra, Eriko Nurvitadhi, Jeffrey J Cook, and Debbie Marr. Wrpn: wide reduced-precision networks. *arXiv preprint arXiv:1709.01134*, 2017.
- [21] Daisuke Miyashita, Edward H Lee, and Boris Murmann. Convolutional neural networks using logarithmic data representation. *arXiv preprint arXiv:1603.01025*, 2016.
- [22] Jeffrey Pennington, Samuel Schoenholz, and Surya Ganguli. Resurrecting the sigmoid in deep learning through dynamical isometry: theory and practice. In *Advances in neural information processing systems*, pages 4785–4795, 2017.
- [23] Ben Poole, Subhaneil Lahiri, Maithra Raghu, Jascha Sohl-Dickstein, and Surya Ganguli. Exponential expressivity in deep neural networks through transient chaos. In *Advances in neural information processing systems*, pages 3360–3368, 2016.
- [24] Mohammad Rastegari, Vicente Ordonez, Joseph Redmon, and Ali Farhadi. Xnor-net: Imagenet classification using binary convolutional neural networks. In *European Conference on Computer Vision*, pages 525–542. Springer, 2016.
- [25] Samuel S Schoenholz, Justin Gilmer, Surya Ganguli, and Jascha Sohl-Dickstein. Deep information propagation. *arXiv preprint arXiv:1611.01232*, 2016.
- [26] Hava T. Siegelmann and Eduardo D. Sontag. Turing computability with neural nets. *Applied Mathematics Letters*, 4(6):77–80, jan 1991.
- [27] Naigang Wang, Jungwook Choi, Daniel Brand, Chia-Yu Chen, and Kailash Gopalakrishnan. Training deep neural networks with 8-bit floating point numbers. In *Advances in neural information processing systems*, pages 7675–7684, 2018.
- [28] Anqi Wu, Sebastian Nowozin, Edward Meeds, Richard E. Turner, Jose Miguel Hernandez-Lobato, and Alexander L. Gaunt. Deterministic variational inference for robust bayesian neural networks. In *International Conference on Learning Representations*, 2019.
- [29] Lechao Xiao, Yasaman Bahri, Jascha Sohl-Dickstein, Samuel S Schoenholz, and Jeffrey Pennington. Dynamical isometry and a mean field theory of cnns: How to train 10,000-layer vanilla convolutional neural networks. *arXiv preprint arXiv:1806.05393*, 2018.
- [30] Ge Yang and Samuel Schoenholz. Mean field residual networks: On the edge of chaos. In *Advances in neural information processing systems*, pages 7103–7114, 2017.
- [31] Penghang Yin, Jiancheng Lyu, Shuai Zhang, Stanley Osher, Yingyong Qi, and Jack Xin. Understanding straight-through estimator in training activation quantized neural nets. *ICLR*, pages 1–30, 2019.
- [32] Chiyuan Zhang, Samy Bengio, Moritz Hardt, Benjamin Recht, and Oriol Vinyals. Understanding deep learning requires rethinking generalization. *arXiv preprint arXiv:1611.03530*, 2016.
- [33] Yiren Zhou, Seyed-Mohsen Moosavi-Dezfooli, Ngai-Man Cheung, and Pascal Frossard. Adaptive quantization for deep neural network. In *Thirty-Second AAAI Conference on Artificial Intelligence*, 2018.

Appendix

A Proof of Lemma 1

Proof of Lemma 1. The dynamical system is given by

$$\begin{pmatrix} Q^{(l)} \\ C^{(l)} \end{pmatrix} = \begin{pmatrix} \sigma_w^2 \mathbb{E}_{u \sim \mathcal{N}(0, Q^{(l-1)})} \phi^2(u) + \sigma_b^2 \\ \frac{1}{Q^{(l-1)}} \left[\sigma_w^2 \mathbb{E}_{(u_1, u_2) \sim \mathcal{N}(0, \Sigma(Q^{(l-1)}, C^{(l-1)})} \phi(u_1)\phi(u_2) + \sigma_b^2 \right] \end{pmatrix} \equiv \mathcal{M} \left[\begin{pmatrix} Q^{(l-1)} \\ C^{(l-1)} \end{pmatrix} \right]. \quad (20)$$

Since $Q^{(l)} = \sigma_w^2 \widehat{Q}^{(l-1)} + \sigma_b^2$, convergence of $Q^{(l)}$ to a fixed point is equivalent to convergence of $\widehat{Q}^{(l)}$. If we assume $Q^{(l)}$ has converged to Q^* , the system in eq. 20 reduces to

$$\mathcal{M}_{Q^*}(C) = \frac{1}{Q^*} \left[\sigma_w^2 \mathbb{E}_{(u_1, u_2) \sim \mathcal{N}(0, \Sigma(Q^*, C))} \phi(u_1)\phi(u_2) + \sigma_b^2 \right] \quad (21)$$

Linearizing the above equation gives

$$\mathcal{M}_{Q^*}(C) = \mathcal{M}_{Q^*}(C^*) + \underbrace{\frac{\partial \mathcal{M}_{Q^*}(C^*)}{\partial C}}_{\equiv \chi} (C - C^*) + O((C - C^*)^2)$$

and using a Cholesky decomposition and denoting by $\mathcal{D}x$ a standard Gaussian measure, we have

$$\begin{aligned} \chi_{C^*} &= \frac{1}{Q^*} \frac{\partial}{\partial C} \left[\sigma_w^2 \mathbb{E}_{(u_1, u_2) \sim \mathcal{N}(0, \Sigma(Q^*, C))} \phi(u_1)\phi(u_2) + \sigma_b^2 \right]_{C=C^*} \\ &= \frac{\sigma_w^2}{Q^*} \int \mathcal{D}z_1 \mathcal{D}z_2 \phi(\sqrt{Q^*}z_1 + \mu_b) \frac{\partial}{\partial C} \phi(\sqrt{Q^*}(Cz_1 + \sqrt{1-C^2}z_2) + \mu_b)_{C=C^*} \\ &= \frac{\sigma_w^2}{Q^*} \int \mathcal{D}z_1 \mathcal{D}z_2 \phi(\sqrt{Q^*}z_1 + \mu_b) \phi'(\sqrt{Q^*}(Cz_1 + \sqrt{1-C^2}z_2) + \mu_b) \sqrt{Q^*} \left(z_1 - \frac{z_2 C}{\sqrt{1-C^2}} \right) \end{aligned}$$

and using $\int \mathcal{D}z g(z)z = \int \mathcal{D}z g'(z)$ which holds for any $g(z)$

$$= \sigma_w^2 \mathbb{E}_{(u_1, u_2) \sim \mathcal{N}(0, \Sigma(Q^*, C))} \phi'(u_1)\phi'(u_2).$$

The time scale of convergence dictated by the rate χ is obtained by solving the linear equation for $\varepsilon^{(l)} = C^{(l)} - C^*$, which gives $\varepsilon^{(l)} = \varepsilon_0 e^{-l/\xi}$ and thus in the linear regime we have

$$e^{-1/\xi} = \frac{\varepsilon^{(l+1)}}{\varepsilon^{(l)}} = \frac{\mathcal{M}_{Q^*}(C^{(l)}) - C^*}{C^{(l)} - C^*} \approx \frac{C^* + \chi(C^{(l)} - C^*) - C^*}{C^{(l)} - C^*} = \chi$$

$$\xi = -\frac{1}{\log \chi}.$$

Since a smooth convex function can intersect a linear function at no more than two points unless the two are equal (since otherwise the gradient must change sign twice implying negative curvature at some point), in order to show that $\mathcal{M}_{Q^*}(C)$ can have at most two fixed points in $[0, 1]$ it suffices to show that it is convex in this range. A calculation similar to the one above gives:

$$\frac{\partial^2 \mathcal{M}_{Q^*}(C)}{\partial C^2} = \sigma_w^2 Q^* \mathbb{E}_{(u_1, u_2) \sim \mathcal{N}(0, \Sigma(Q^*, C))} \phi''(u_1)\phi''(u_2).$$

If ϕ is odd, so is ϕ'' and then the expression above is non-negative for $C \in [0, 1]$ according to Lemma 2 in [8]. It is obviously also non-negative simply if ϕ'' is uniformly non-negative. The result applies to

quantized activation as well since we can replace the Heaviside function with a smooth approximation that is identical to within machine precision, and apply the above argument.

Since a fixed point is only stable if the slope χ is smaller than 1 and there are at most two fixed points in $[0, 1]$, there can be at most one stable fixed point. It follows that the fixed point of the dynamics does not depend on initialization as long as $C^{(0)} \geq 0$. While there may be another stable fixed point in $[-1, 0)$, the network will still be unable to distinguish between any two inputs that are either completely uncorrelated or positively correlated, which will generally prevent learning aside from trivial tasks where data points in different classes are always negatively correlated, and thus the data is linearly separable. \square

B Covariances of post-activations

In the main text we review results on asymptotic normality of pre-activations $\alpha^{(l)}(x)$ of deep feed-forward networks at the infinite width limit. The analysis of signal propagation in such networks is based on studying convergence of the covariances of these pre-activations to their fixed points. The convergence rate in eq. 6 and the corresponding time scale in eq. 7 that gives the typical maximal trainable depth are thus the main objects of interest.

It will be convenient at times to consider instead the evolution of the covariances of the post-activations $\hat{\alpha}^{(l)}(x) = \phi(\alpha^{(l)}(x))$. We do this by defining, analogously to eq. 3,

$$\begin{pmatrix} \mathbb{E}\hat{\alpha}_i^{(l)}(x)\hat{\alpha}_i^{(l)}(x) & \mathbb{E}\hat{\alpha}_i^{(l)}(x)\hat{\alpha}_i^{(l)}(x') \\ \mathbb{E}\hat{\alpha}_i^{(l)}(x)\hat{\alpha}_i^{(l)}(x') & \mathbb{E}\hat{\alpha}_i^{(l)}(x')\hat{\alpha}_i^{(l)}(x') \end{pmatrix} = \begin{pmatrix} \hat{\Sigma}^{(l)}(x, x) & \hat{\Sigma}^{(l)}(x, x') \\ \hat{\Sigma}^{(l)}(x, x') & \hat{\Sigma}^{(l)}(x', x') \end{pmatrix} = \hat{Q}^{(l)} \begin{pmatrix} 1 & \hat{C}^{(l)} \\ \hat{C}^{(l)} & 1 \end{pmatrix} \quad (22)$$

For a given x, x' the quantities $Q^{(l)}, C^{(l)}$ are trivially related to $\hat{Q}^{(l-1)}, \hat{C}^{(l-1)}$ via eq. 2, which gives

$$Q^{(l)} = \sigma_w^2 \hat{Q}^{(l-1)} + \sigma_b^2$$

$$C^{(l)} = \frac{\sigma_w^2 \hat{Q}^{(l-1)} \hat{C}^{(l-1)} + \sigma_b^2}{Q^{(l)}}.$$

The covariance map for the hidden states analogous to eq. 5 is simply

$$\widehat{\mathcal{M}}_{\hat{Q}^*}(\hat{C}) = \frac{1}{\hat{Q}^*} \mathbb{E}_{(u_1, u_2) \sim \mathcal{N}(0, \hat{\Sigma}(\hat{Q}^*, \hat{C}))} \phi(u_1)\phi(u_2) \quad (23)$$

where $\hat{\Sigma}(\hat{Q}^*, \hat{C}) = \begin{pmatrix} \sigma_w^2 \hat{Q}^* + \sigma_b^2 & \sigma_w^2 \hat{Q}^* \hat{C} + \sigma_b^2 \\ \sigma_w^2 \hat{Q}^* \hat{C} + \sigma_b^2 & \sigma_w^2 \hat{Q}^* + \sigma_b^2 \end{pmatrix}$. The convergence rates for 5 are identical since

$$\begin{aligned} \frac{\partial \mathcal{M}_{Q^*}(C^{(l)})}{\partial C^{(l)}} &= \frac{\partial C^{(l+1)}}{\partial C^{(l)}} = \frac{1}{Q^*} \frac{\partial (\sigma_w^2 \hat{C}^{(l)} + \sigma_b^2)}{\partial C^{(l)}} \\ &= \frac{1}{Q^*} \frac{\partial \sigma_w^2 \hat{C}^{(l)} + \sigma_b^2}{\partial \hat{C}^{(l-1)}} \frac{\partial \hat{C}^{(l-1)}}{\partial C^{(l)}} = \frac{\partial \hat{C}^{(l)}}{\partial \hat{C}^{(l-1)}} = \frac{\partial \widehat{\mathcal{M}}_{\hat{Q}^*}(\hat{C}^{(l-1)})}{\partial \hat{C}^{(l-1)}} \end{aligned}$$

giving

$$\chi = \lim_{l \rightarrow \infty} \frac{\partial \mathcal{M}_{Q^*}(C^{(l)})}{\partial C^{(l)}} = \lim_{l \rightarrow \infty} \frac{\partial \widehat{\mathcal{M}}_{\hat{Q}^*}(\hat{C}^{(l-1)})}{\partial \hat{C}^{(l-1)}} = \hat{\chi}.$$

C Calculation of the fixed point slope for sign-activation

For convenience, we use the hidden states covariances and mapping $\hat{C}, \hat{Q}, \widehat{\mathcal{M}}$ as defined in appendix B, as they have a linear relationship to the pre-activation at the fixed point. Using a Cholesky

decomposition on the equation 10: $\chi = 4\sigma_w^2 \mathbb{E}_{(u_a, u_b) \sim \mathcal{N}(0, \Sigma(Q^*, C^*))} \delta(u_a)\delta(u_b)$, we get

$$4\sigma_w^2 \int_{u_1} \int_{u_2} \frac{1}{2\pi} \exp\left(-\frac{u_1^2 + u_2^2}{2}\right) \delta(\sqrt{Q^*}u_1) \delta\left(\sqrt{Q^*}\left(C^*u_1 + \sqrt{1-(C^*)^2}u_2\right)\right) du_1 du_2.$$

The delta functions enforces: $u_1 = 0, \mu_2 = 0$, giving us

$$\chi = \frac{2}{\pi} \frac{\sigma_w^2}{Q^* \sqrt{1-(C^*)^2}}.$$

Then, using $Q^* = \sigma_w^2 \widehat{Q}^* + \sigma_b^2$, and since $\widehat{Q}^* = 1$ for sign activation:

$$\chi = \frac{2}{\pi} \frac{\sigma_w^2}{(\sigma_w^2 + \sigma_b^2) \sqrt{1-(C^*)^2}}.$$

While this equation is written for the fixed point C^* , this equation can describe the slope of $\mathcal{M}(C)$ for every value of C . Rather than directly calculating $\mathcal{M}(C)$ using equation 4, it is surprisingly time saving to calculate it by using our expression for $\chi(C) = \frac{d\mathcal{M}(C)}{dC}$:

$$\mathcal{M}(C) - \text{const} = \int_0^C \chi(C') dC' = \frac{2}{\pi} \frac{\sigma_w^2}{(\sigma_w^2 + \sigma_b^2)} \arcsin(C).$$

We know that $\mathcal{M}(C = 1) = 1$, from which we can compute the constant

$$\text{const} = \mathcal{M}(1) - \frac{2}{\pi} \frac{\sigma_w^2}{(\sigma_w^2 + \sigma_b^2)} \arcsin(1) = \frac{\sigma_b^2}{\sigma_w^2 + \sigma_b^2}.$$

In conclusion:

$$\mathcal{M}(C) = \frac{\frac{2\sigma_w^2}{\pi} \arcsin(C) + \sigma_b^2}{\sigma_w^2 + \sigma_b^2}$$

It's also worth noting that for the hidden-states, the mapping for sign activation is:

$$\widehat{\mathcal{M}}(\widehat{C}) = \frac{2}{\pi} \arcsin\left(\frac{\widehat{C}\sigma_w^2 + \sigma_b^2}{\sigma_w^2 + \sigma_b^2}\right)$$

D Stochastic Rounding

One possible way to counter the negative effects of quantization which has proven itself in the past, is by adding noise to the rounding process. Being a commonplace method in machine learning, we would like to explore the effects of stochastic rounding on the dynamics of the neural network. When using this method the sign activation becomes probabilistic and can be modeled as:

$$\phi(x) = \text{sign}(x + n) \tag{24}$$

when $n \sim \text{Uniform}[-1, 1]$ is randomized for every neuron. Rather than working with a uniformly distributed noise, we replace it with a normal-distributed noise. Therefore, $\phi(u) = \text{sign}(u + n)$, for $n \sim \mathcal{N}(0, a^2)$. We justify this using a numeric simulation presented in figure 4, and in Appendix D.1 we find that the expression for stochastic rounding mapping (for hidden states) $\widehat{\mathcal{M}}_{sr}(\widehat{C})$ is:

$$\widehat{\mathcal{M}}_{sr}(\widehat{C}) = \frac{2}{\pi} \arcsin\left(\frac{1}{B} \frac{\widehat{C}\sigma_w^2 + \sigma_b^2}{\sigma_w^2 + \sigma_b^2}\right) \tag{25}$$

where $B = \sqrt{1 + \left(\frac{a}{Q^*}\right)^2 (2Q^* + a^2)}$. While the new mapping function for \widehat{C} does not reach infinite slope at any point (since $C \leq 1, B > 1$), the noise also eliminates $\widehat{C} = 1$ as a fixed point. This result is consistent with the findings of [25] who have shown a similar phenomena when using dropout. Due to the arcsin function being a convex, monotonically increasing function in the area $0 < C < 1$,

We can also conclude that adding noise (and therefore, increasing B) can only decrease the fixed point slope. See K.2 for proof, and figure 4 for illustration.

D.1 Development of the mean field equations for stochastic rounding

We now want to use the stochastic sign activation function to evaluate how it effects the $\widehat{\mathcal{M}}(C)$. Using equation 6, and we get:

$$\chi = 4\sigma_w^2 \int_{-\infty}^{\infty} dn_1 \int_{-\infty}^{\infty} dn_2 \int_{-\infty}^{\infty} du_1 \int_{-\infty}^{\infty} du_2 \frac{1}{2\pi} \frac{1}{2\pi a^2} \exp\left(-\frac{n_1^2}{2a^2}\right) \exp\left(-\frac{n_2^2}{2a^2}\right) \exp\left(-\frac{u_1^2}{2}\right) \exp\left(-\frac{u_2^2}{2}\right) \delta\left(\sqrt{Q^*}u_1 + n_1\right) \delta\left(\sqrt{Q^*}\left(Cu_1 + \sqrt{1-(C)^2}u_2\right) + n_2\right)$$

We use the delta functions to enforce: $u_1 = -\frac{n_1}{\sqrt{Q^*}}$, $u_2 = -\frac{n_2 - C(n_1)}{\sqrt{Q^*}\sqrt{1-(C)^2}}$ and get:

$$\chi = \frac{2\sigma_w^2}{\pi Q^* a^2 \sqrt{1-(C)^2}} \frac{1}{2\pi} \int_{-\infty}^{\infty} \int_{-\infty}^{\infty} \exp\left(-\frac{n_1^2}{2a^2}\right) \exp\left(-\frac{n_2^2}{2a^2}\right) \exp\left(-\frac{(n_1)^2}{2Q^*}\right) \exp\left(-\frac{(n_2 - C(n_1))^2}{2Q^*(1-(C)^2)}\right) dn_1 dn_2 \quad (26)$$

Which can otherwise be written as:

$$\frac{2\sigma_w^2}{\pi Q^* a^2 \sqrt{1-(C)^2}} \frac{1}{2\pi} \int_{-\infty}^{\infty} \int_{-\infty}^{\infty} \exp\left[-\frac{1}{2}D\right] dn_1 dn_2$$

$$D = \frac{n_1^2 (1-(C)^2) (a^2 + (Q^*)^2) + n_2^2 Q^* (1-(C)^2) + a^2 n_2^2 - 2a^2 n_1 n_2 C + a^2 n_1^2 (C)^2}{Q^* (1-(C)^2) a^2}$$

So:

$$\chi = \frac{2\sigma_w^2}{\pi Q^* a^2 \sqrt{1-(C)^2}} \frac{1}{2\pi} \int_{-\infty}^{\infty} \int_{-\infty}^{\infty} \exp\left[-\frac{1}{2} \frac{1}{Q^* (1-(C)^2) a^2} \begin{pmatrix} n_1 & n_2 \end{pmatrix} \Sigma^{-1} \begin{pmatrix} n_1 \\ n_2 \end{pmatrix}\right] dn_1 dn_2 \quad (27)$$

$$\Sigma^{-1} = \begin{pmatrix} (1-(C)^2) a^2 + (1-(C)^2) (Q^*)^2 + a^2 (C)^2 & -a^2 C \\ -a^2 C & Q^* (1-(C)^2) + a^2 \end{pmatrix}$$

Solving the Gaussian we get:

$$|\Sigma|^{-1} = |\Sigma^{-1}| = \frac{(Q^* (1-(C)^2) + a^2)^2 - (a^2 C)^2}{(Q^* (1-(C)^2) a^2)^2} = \quad (28)$$

$$\frac{(Q^*)^2 (1-(C)^2)^2 + 2a^2 Q^* (1-(C)^2) + a^4 - a^4 (C)^2}{(Q^* (1-(C)^2) a^2)^2} =$$

$$\frac{(Q^*)^2 (1-(C)^2)^2 + a^2 (2Q^* + a^2) (1-(C)^2)}{(Q^*)^2 (1-(C)^2)^2 a^4}$$

Resulting:

$$\chi = \frac{2\sigma_w^2}{\pi Q^* a^2 \sqrt{1-(C)^2}} \frac{1}{2\pi} (2\pi \sqrt{|\Sigma|}) = \frac{2\sigma_w^2}{\pi Q^* a^2 \sqrt{1-(C)^2}} \sqrt{\frac{(Q^*)^2 (1-(C)^2) a^4}{(Q^*)^2 (1-(C)^2) + a^2 (2Q^* + a^2)}} \quad (29)$$

And we finally get:

$$\chi = \frac{2\sigma_w^2}{\pi Q^* \sqrt{(1-(C)^2) + \left(\frac{a}{Q^*}\right)^2 (2Q^* + a^2)}}$$

For the rest of this section, We will use the shortcut $B \equiv \sqrt{1 + \left(\frac{a}{Q^*}\right)^2 (2Q^* + a^2)}$ We can now write the equation as:

$$\chi = \frac{2\sigma_w^2}{\pi Q^* \sqrt{\left(1 - \left(\frac{C}{B}\right)^2\right)}} \quad (30)$$

for $x = \frac{C^*}{B}, \frac{dC}{dx} = B$

$$\widehat{\mathcal{M}}(\widehat{C}) = \int \frac{d\widehat{\mathcal{M}}(\widehat{C})}{d\widehat{C}} d\widehat{C} = \int \frac{d\widehat{\mathcal{M}}(C)}{dC} \frac{d\widehat{C}}{dC} dC = \int \chi \frac{d\widehat{C}}{dC} \frac{dC}{dx} dx$$

When we again drop the constant so $\widehat{\mathcal{M}}(\widehat{C} = 1) = 1$, and get:

$$\widehat{\mathcal{M}}(\widehat{C}) = \frac{2}{\pi} \arcsin\left(\frac{C}{B}\right) \quad (31)$$

Based on this equation, we can also use a Taylor expansion, to estimate \widehat{C}^* , and we get the solution:

$$\widehat{C}^* \simeq 1 - \frac{4}{\pi^2} \frac{\sigma_w^2}{Q^* B} \left(1 + \sqrt{1 + \left(\frac{\pi}{2}\right)^4 (B^2 - B) \left(\frac{Q^*}{\sigma_w^2}\right)^2}\right) \quad (32)$$

E Calculations of $Q^{(l)}$ and χ for general quantized activations

We start by evaluating \widehat{Q} , the hidden-state covariance (see appendix B) for the general quantization activation function defined in 13, using equation 22

$$\widehat{Q}^{(l)} = \mathbb{E}_{u \sim \mathcal{N}(0, Q^{(l)})} \left(A + \sum_{i=1}^{N-1} H(u - g_i) h_i \right)^2 - \left(\mu^{(l)} \right)^2,$$

where:

$$\mu^{(l)} = \mathbb{E}_{u \sim \mathcal{N}(0, Q^{(l)})} \left(A + \sum_{i=1}^{N-1} H(u - g_i) h_i \right) = A + \sum_{i=1}^{N-1} h_i \Psi\left(-\frac{g_i}{\sqrt{Q^{(l)}}}\right). \quad (33)$$

Here, we use Ψ as the normal cumulative distribution function. The constant A cancels out, and we can expand the multiplication:

$$\widehat{Q}^{(l)} = \sum_{i=1}^{N-1} \sum_{j=1}^{N-1} h_i h_j \left(\mathbb{E}[H(u - g_i) H(u - g_j)] - \Psi\left(-\frac{g_i}{\sqrt{Q^{(l)}}}\right) \Psi\left(-\frac{g_j}{\sqrt{Q^{(l)}}}\right) \right),$$

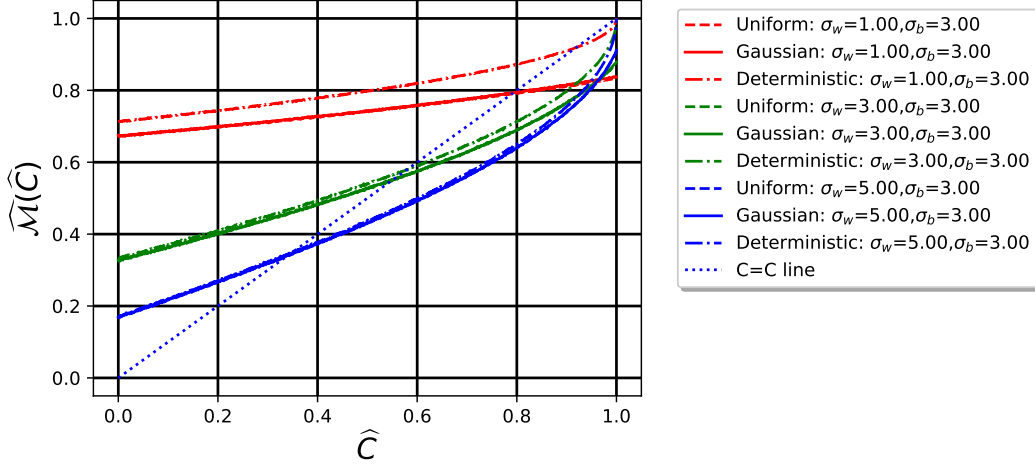


Figure 4: A simulation comparing $\widehat{\mathcal{M}}(\widehat{C})$ for deterministic and stochastic sign activations. For the Gaussian noise, we used the distribution $\mathcal{N}(0, \frac{1}{3})$, so both Gauss and Uniform stochastic activations have the same first and second moments. In all cases, the stochastic activation with the Gauss noise was indistinguishable from the one with the uniform noise.

And since $H(u - g_i)H(u - g_j) = H(u - g_{\max(i,j)})$

$$\widehat{Q}^{(l)} = \sum_{i=1}^{N-1} \sum_{j=1}^{N-1} h_i h_j \left(\Psi \left(-\frac{\max(g_i, g_j)}{\sqrt{Q^{(l)}}} \right) - \Psi \left(-\frac{g_i}{\sqrt{Q^{(l)}}} \right) \Psi \left(-\frac{g_j}{\sqrt{Q^{(l)}}} \right) \right). \quad (34)$$

$\Psi(-x)\Psi(-y) = \Psi(-\max(x, y))\Psi(-\min(x, y))$, so we can see that:

$$\Psi(-\max(x, y)) - \Psi(-x)\Psi(-y) = \Psi(-\max(x, y))(1 - \Psi(-\min(x, y)))$$

And by using the CDF property $\Psi(-x) = 1 - \Psi(x)$, we get

$$\widehat{Q}^{(l)} = \sum_{i=1}^{N-1} \sum_{j=1}^{N-1} h_i h_j \Psi \left(-\frac{\max(g_i, g_j)}{\sqrt{Q^{(l)}}} \right) \Psi \left(\frac{\min(g_i, g_j)}{\sqrt{Q^{(l)}}} \right), \quad (35)$$

from which we can easily compute $Q^{(l+1)}$. In Appendix F, we develop an approximation for $\mathcal{M}(\widehat{C})$. However, for our more immediate concerns, we will go straight to evaluating the equation for the fixed point slope, from eq. 6:

$$\begin{aligned} \chi &= \sigma_w^2 \sum_{i=1}^{N-1} \sum_{j=1}^{N-1} \iint_{u_1, u_2 \sim \mathcal{N}(0, \Sigma(Q^*, C^*))} \exp[-\frac{1}{2}u_1^2] \exp[-\frac{1}{2}u_2^2] h_i h_j \\ &\quad \delta(\sqrt{Q^*}u_1 - g_i) \delta\left(\sqrt{Q^*}\left(C^*u_1 + \sqrt{1 - (C^*)^2}u_2\right) - g_j\right) = \\ &\quad \frac{2\sigma_w^2}{\pi\sqrt{Q^*}} \sum_{i=1}^{N-1} \sum_{j=1}^{N-1} \int \exp\left[-\frac{1}{2}\frac{g_i^2}{Q^*}\right] \exp\left[-\frac{1}{2}u_2^2\right] h_i h_j \\ &\quad \delta\left(\sqrt{Q^*}\left(C^*\frac{g_i}{\sqrt{Q^*}} + \sqrt{1 - (C^*)^2}u_2\right) - g_j\right) = \\ &\quad \frac{2\sigma_w^2}{\pi Q^* \sqrt{1 - (C^*)^2}} \sum_{i=1}^{N-1} \sum_{j=1}^{N-1} \exp\left[-\frac{1}{2}\frac{g_i^2}{Q^*}\right] \exp\left[-\frac{1}{2}\frac{(g_j - C^*g_i)^2}{Q^*(1 - (C^*)^2)}\right] h_i h_j \end{aligned}$$

which can be simplified to:

$$\chi = \frac{2\sigma_w^2}{\pi Q^* \sqrt{1 - (C^*)^2}} \sum_{i=1}^{N-1} \sum_{j=1}^{N-1} h_i h_j \exp\left[-\frac{g_i^2 - 2C^*g_i g_j + g_j^2}{2Q^*(1 - (C^*)^2)}\right]. \quad (36)$$

F The general quantized activations mapping- Approximation and numeric evaluation

F.1 The covariance mapping of a general quantized activation

We once again use the hidden states covariances \widehat{Q}, \widehat{C} Using eq. 5 for general quantized activation, we get the expression:

$$\widehat{C}^{(l)} \widehat{Q}^{(l)} = \mathbb{E}_{u_1, u_2 \sim \mathcal{N}(0, \Sigma(Q^{(l)}, C^{(l)}))} \left(\sum_{i=1}^{N-1} h_i H(u_1 - g_i) - A \right) \left(\sum_{i=1}^{N-1} h_i H(u_2 - g_j) - A \right) - (\mu^{(l)})^2,$$

where we can use eq. 33 and expand it to:

$$\widehat{C}^{(l)} \widehat{Q}^{(l)} = \sum_{i=1}^{N-1} \sum_{j=1}^{N-1} \left(\mathbb{E}_{u_1, u_2 \sim \mathcal{N}(0, \Sigma(Q^{(l)}, C^{(l)}))} [H(u_1 - g_i) H(u_2 - g_j)] - \Psi\left(\frac{-g_i}{\sqrt{Q^{(l)}}}\right) \Psi\left(\frac{-g_j}{\sqrt{Q^{(l)}}}\right) \right).$$

When the offsets are different than zero, there is no exact solution for the expectancy when u_1, u_2 are correlated. Article [28] suggests an approximation for finding $\widehat{\mathcal{M}}(\widehat{C})$, when $C(\widehat{C}) = \frac{Q^* C \sigma_w^2 + \sigma_b^2}{Q^* \sigma_w^2 + \sigma_b^2}$:

$$\widehat{\mathcal{M}}(\widehat{C}) \simeq \frac{\arcsin(C^*)}{2\pi Q^*} \sum_{i=1}^{N-1} \sum_{j=1}^{N-1} h_i h_j \cdot \exp\left(-\frac{1}{2} \frac{C}{\arcsin(C) Q^* \sqrt{1-C^2}} \left(g_i^2 + g_j^2 - g_i g_j \frac{2C}{1+\sqrt{1-C^2}}\right)\right) \quad (37)$$

We found the approximation to hold well in the area $C \sim 0$, and $\forall i, g_i < Q^*$. Therefore, when Q^* is known, this equation can be used to evaluate C^* with reduced complexity.

F.2 Quick numeric method to approximate the fixed point slope, for $\sigma_b > 0$

Using eq. 37, we suggest a numeric algorithm to evaluate the fixed point slope for $\sigma_b > 0$, for any quantized activation function:

1. Evaluate Q by iterative usage of eq. 14. Start with arbitrary value $\widehat{Q} = 1.0$ and repeat T times.
2. Use eq. 37 to evaluate $\widehat{\mathcal{M}}(\widehat{C} = 0)$ (Reminder: $C(\widehat{C} = 0) = \frac{\sigma_b^2}{Q \sigma_w^2 + \sigma_b^2}$)
3. Use eq. 15 to evaluate $\chi(\widehat{C} = 0)$
4. Estimate \widehat{C}^* by $\frac{C(\widehat{C}=0)}{1-\chi(\widehat{C}=0)}$ (First order approximation), and use equation 15 to find the fixed point slope.

We found this algorithm to be very efficient and accurate when studying the dynamics in the area of $\sigma_b > 0$. Results of using this estimation are displayed in figure 5.

G Beyond constant-spaced quantized activations

Our main focus in this article, have been the quantized activations with constant spacing. We now want to study the effects of using more complex activation functions on the dynamics of the network. We will do so by defining a new family of quantized activation functions, the linear-spacing activations- For any given values of $h, c_1 > 0, c_2 \in \mathbb{R}$, the function parameters in accordance with equation 13, are:

$$\forall i \in \{1, \dots, N-1\}, m \equiv \left(k - \frac{N}{2} - 2\right), h_i = h, \quad \tilde{g}_i = \tilde{D}_0 m \left(1 + \tilde{D}_1 |m|\right) \quad (38)$$

This family of functions can be thought of a second order generalization of the constant-spaced functions, which correspond to the special case $\tilde{D}_1 = 0$. This family of functions is important, as it also includes sigmoid-like quantized activation functions (given for values of $\tilde{D}_1 > 0$). To evaluate the dynamics of the new family, we again use eq. 16 and the depth scale definition eq. 7, and run a grid search over the normalized values of \tilde{D}_1, \tilde{D}_0 , calculating the depth scale for each combination

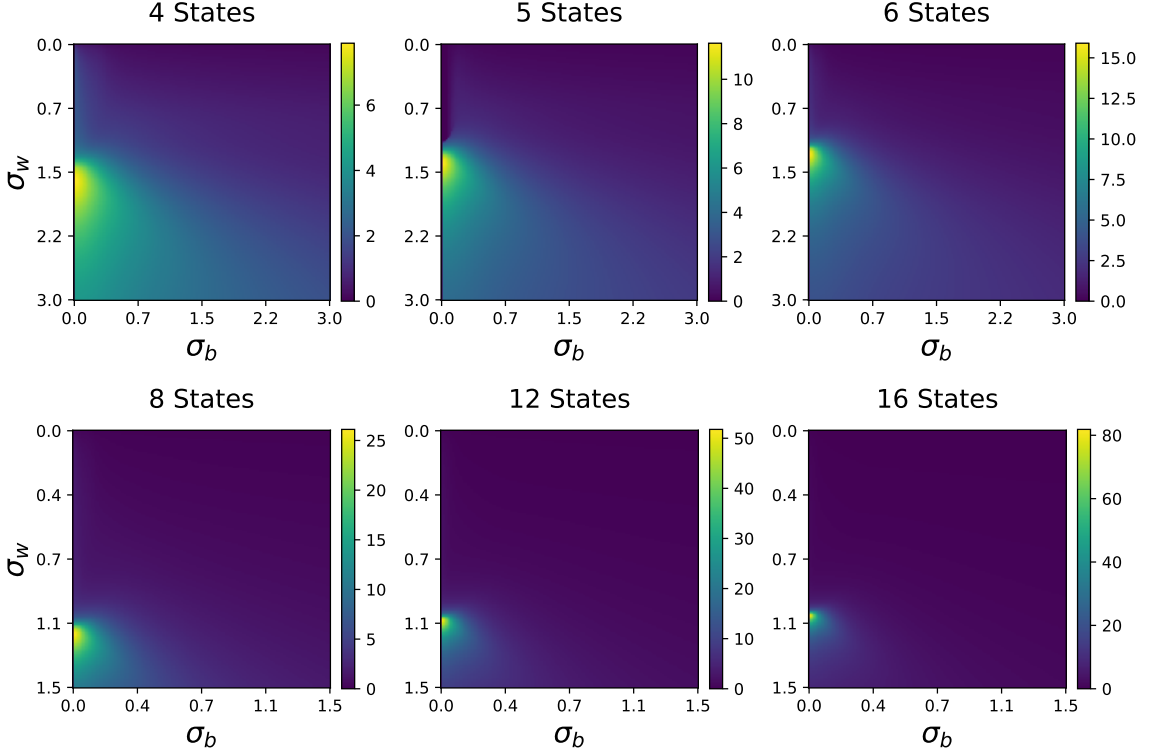


Figure 5: Grid-Approximation of the depth scale ξ for constant-spaced activations of different quantization levels, as a function of the initialization parameters. $D = 1$ was used as the constant space between offsets. For this approximation, we used the algorithm described in F.2. It is apparent that the maximal depth scale for all quantization levels is achievable for $\sigma_b \simeq 0$.

of parameters. The results of the grid search for several different quantization levels are presented in Figure 6. In all of the tested activations, the maximal depthscale that we found was identical, within numeric error range, to the maximal depthscale found for constant-spaced activations, indicating that the additional degree of freedom does not help improving the dynamical properties of the activation. A more in-depth study of the grid search does show that the optimum value can be achieved for linear-spaced activations ($\tilde{D}_1 = 0$), while the additional linear-shaped peaks suggest that using some sigmoids-like quantized activations ($\tilde{D}_1 > 0$), Characterized by specific ratios $\frac{\tilde{D}_1}{\tilde{D}_0} = \frac{D_1}{D_0}$, can also result optimal or near optimal depth-scale.

H Additional MNIST training-results

When studying the empirical effects of the initialization parameters on trainability when using a 10 states quantization, and seen that the longest trainable network is achieved when using the \tilde{D}_{opt} , the optimal normalized distance between offsets, as proposed by our theory. Additional test have been made to other quantization levels as well and gave similar results. It is unclear from the results, however, whether the degradation of deep networks is caused by the unoptimized propagation of the forward pass, or by the unoptimized backward pass. To isolate the effects of the forward pass which are of more interest to us, we measured the effects of σ_w on a 10 states quantization once more, but optimized the STE to allow clean gradient propagation using $\rho^{-1} = \sigma_w \sqrt{\text{erf}\left(\frac{1}{\sqrt{2}Q^*}\right)}$, when using σ_w and Q^* based on each run's initialization values. Figure 7 shows the results of this experiment, and confirms that the optimal initialization is dominated by the forward pass.

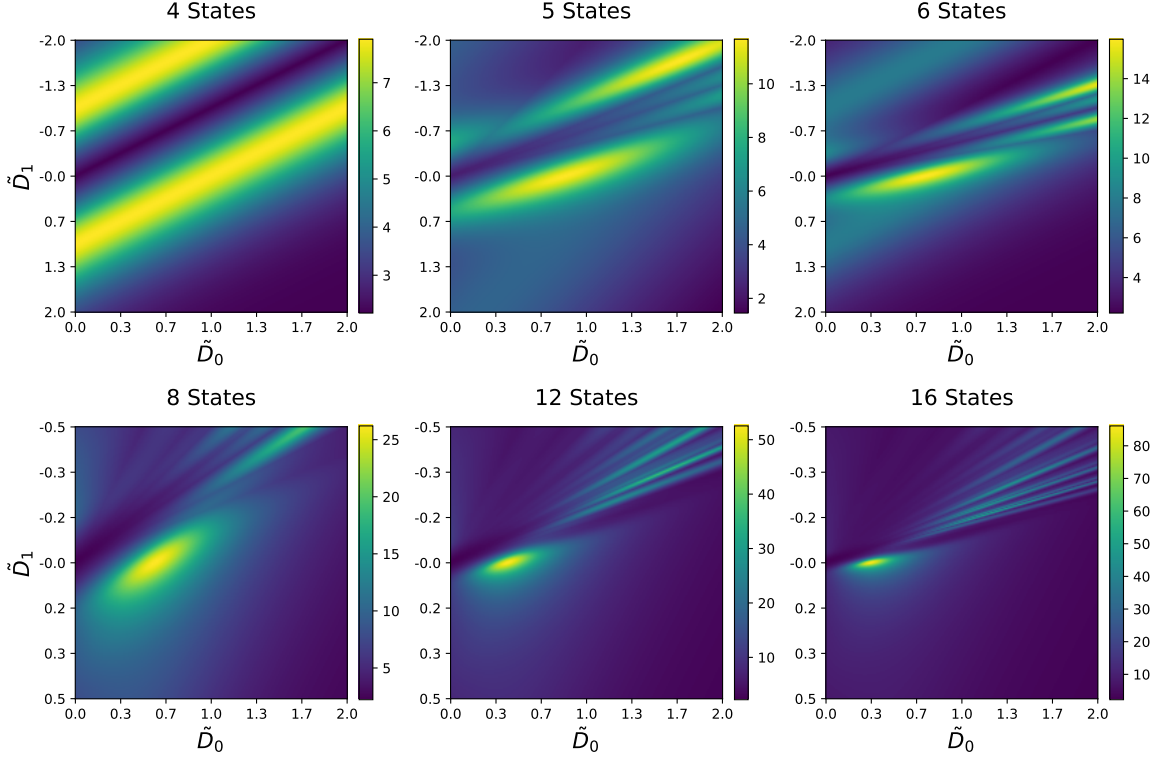


Figure 6: Evaluation of the depth scale ξ for linear-spaced quantized activation, with the initialization $\sigma_b = 0$. The search resolution is 1000×1000 for each quantization level. The maximum depth-scale on each grid for square spacing activations is always achievable for the constant spacing as well, where $\tilde{D}_1 = 0$.

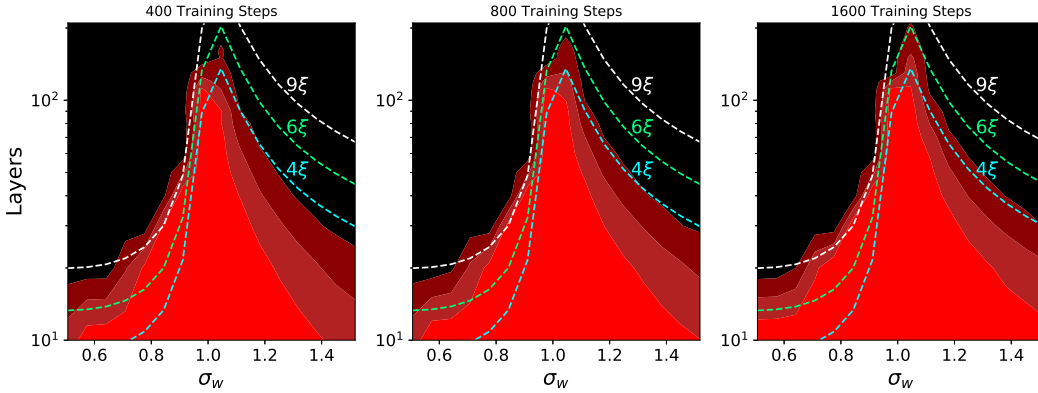


Figure 7: Test accuracy of a 10-states activation in feed-forward network, over the MNIST data-set, with different initialization values and optimized STE for backward propagation of gradients. When compared with the 3, we can see that adjusting the networks for better backward propagation of the gradients does not have a significant effect on the trainability of deep networks.

I Simplified Optimization of the initialization parameters

Sections 4 describes an algorithm for computation of the value of the initialization parameter σ_w , that would allow the best signal propagation in the network for any quantized activation function.

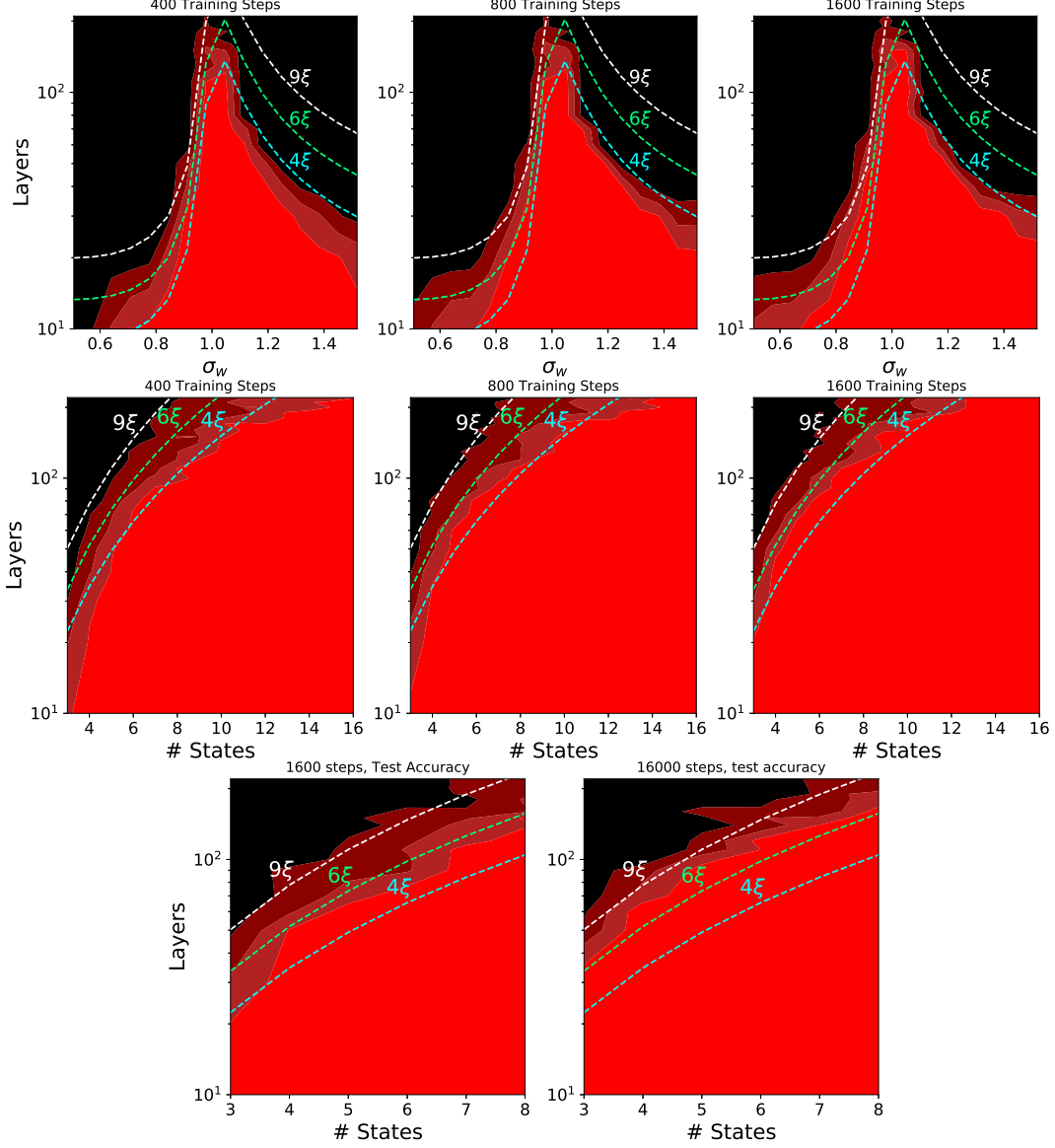


Figure 8: Time evolution of the test accuracy. Line 1&2: The evolution of the heat maps presented in figure 3, at an early stage of training (Training accuracy) . Bottom line: Test accuracy at the initial stage (1600 steps) and at an advanced stage of the run (16000 steps), focused on networks with more layers than their corresponding depth-scale. Those results align with the results of [25], showing that even in an advanced stage of training, networks with layers exceeding $\sim 6\xi$ are untrainable.

However, when dealing with the constant spaced activation functions of the form:

$$\phi_N(x) = -1 + \sum_{i=1}^{N-1} \frac{2}{N-1} H\left(x - \frac{2}{N-1} \left(i - \frac{N}{2}\right)\right),$$

we find that our suggested method of initialization quickly converges to the *Xavier initialization* [9], as the quantization levels increases. For simple initialization, we suggest a small modification for the Xavier method that accounts for quantization: When F_{in} and F_{out} are the fan-in and fan-out of the layer, rather than simply computing the standard error for weights initialization using

$\sigma_w = \sqrt{\frac{2}{F_{in} + F_{out}}}$ as in the case of normal Xavier, we suggest that using a factor of

$$\alpha_N = 1 + \frac{1.23}{(N + 0.2)^2}$$

(when N is the number of activation states), so that:

$$\sigma_w = \alpha_N \cdot \sqrt{\frac{2}{F_{in} + F_{out}}}$$

We see that for the continuous case, our activation function becomes hard-tangent and our factor becomes $\lim_{N \rightarrow \infty} \alpha_N = 1$. α_N was estimated by computing the value σ_w that ensures $\frac{D}{\sqrt{Q}} = \tilde{D}_{\text{opt}}$ for states ranging from 1 to 128, and fitting the results $\sigma_w(N)$ to the function $1 + \frac{a}{(N-b)^2}$, which behaved accordingly. For the case where the number of states is larger than 128, the factor α_N is small enough for the error to be irrelevant. Figure 10 shows a comparison between the standard Xavier and our modified initialization for 3-states activation, where α_N is at it's peak.

J Backwards signal propagation for straight through estimator

While we use quantized activations for the forward pass, the backward propagation of quantized neural networks is, in our case, done by straight through estimators (STE). When using constant-spaced quantized activations, we choose a STE to imitate the backward pass of the hard-tanh function:

$$\phi_\rho(x) = \begin{cases} -\rho^{-1} & x < -1 \\ x\rho & -1 \leq x \leq 1 \\ \rho^{-1} & x > 1 \end{cases}$$

where $\rho > 0$ is a parameter that controls the slope of the hard-tanh, so the backward equation is determined by the derivative:

$$\phi'_\rho(x) = \begin{cases} \rho & |x| < 1 \\ 0 & \text{else} \end{cases} \quad (39)$$

The moments of a random $N \times N$ matrix $\bar{\mathbf{A}}$ are given by $m_{\bar{\mathbf{A}}}^{(i)} = \frac{1}{N} \mathbb{E} \text{tr} (\bar{\mathbf{A}}^i)$. In the case of eq. 9, and our STE ϕ_ρ , the equation is reduced to

$$m_{\mathbf{J}\mathbf{J}^T}^{(1)} = \frac{1}{N} \mathbb{E} \text{tr} (\phi'_\rho(\mathbf{u}^*) \mathbf{W} (\phi'_\rho(\mathbf{u}^*) \mathbf{W}))$$

where $u_i^* \sim \mathcal{N}(0, Q^*)$.i.d and $\mathbf{D}_{\phi'(\mathbf{u}^*)}$ is a diagonal matrix with $\phi'(\mathbf{u}^*)$ on the diagonal. This gives

$$m_{\mathbf{J}\mathbf{J}^T}^{(1)} = \sigma_w^2 \int (\phi'_\rho(\sqrt{Q^*}z))^2 \mathcal{D}z$$

where $\mathcal{D}z = \frac{1}{\sqrt{2\pi}} \exp\left(\frac{-z^2}{2}\right)$. Then obtain:

$$m_{\mathbf{J}\mathbf{J}^T}^{(1)} = \sigma_w^2 \rho^2 \int_{-1/\sqrt{Q^*}}^{1/\sqrt{Q^*}} \mathcal{D}u = \sigma_w^2 \rho^2 \text{erf}\left(\frac{1}{\sqrt{2Q^*}}\right). \quad (40)$$

Assuming we already have the value σ_w, Q^* , we can set $\rho^{-1} = \sigma_w \sqrt{\text{erf}\left(\frac{1}{\sqrt{2Q^*}}\right)}$ to ensure $m_{\mathbf{J}\mathbf{J}^T} = 1$, and thus avoid vanishing and exploding gradients.

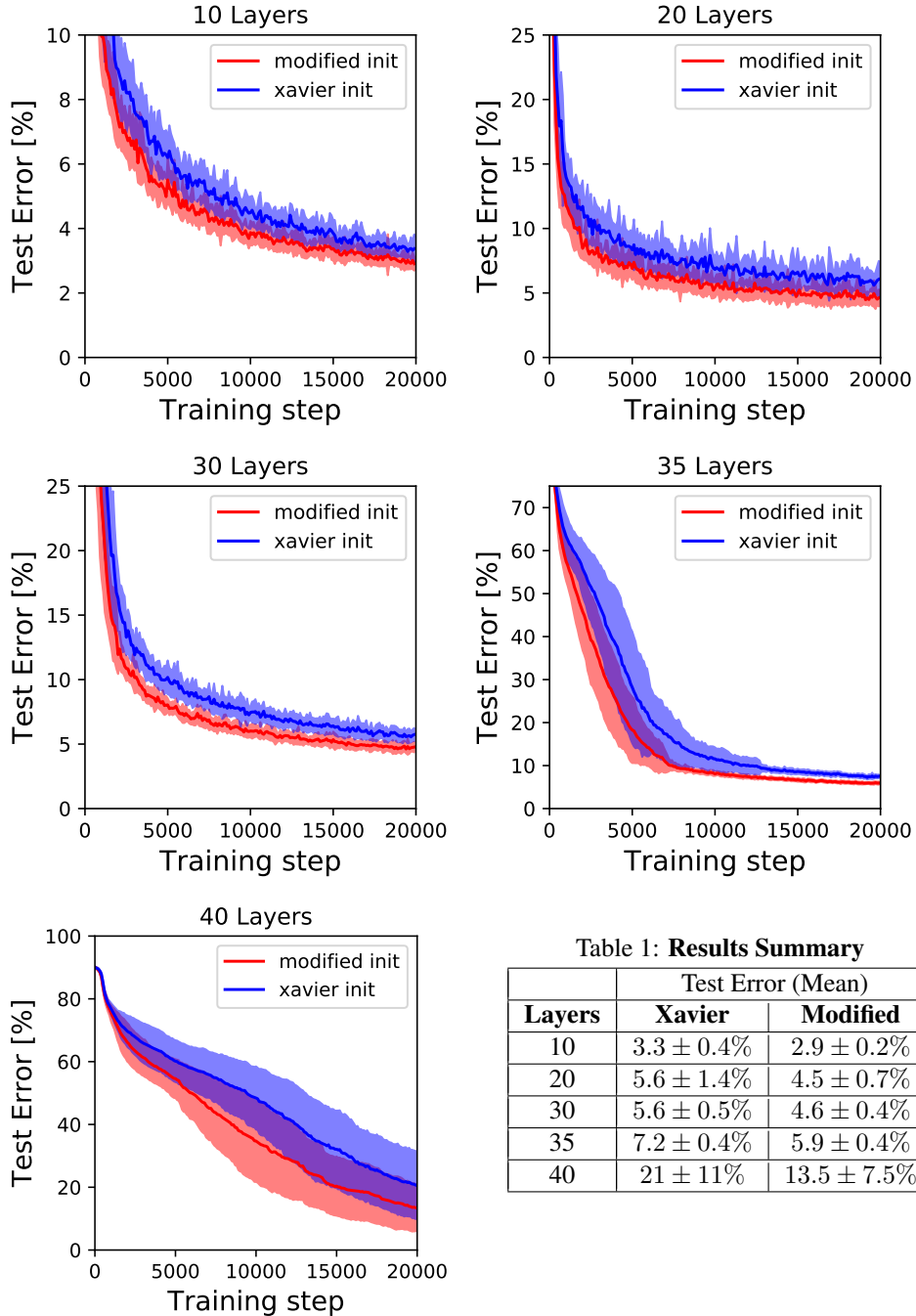


Figure 10: Comparison of our suggested initialization with the Xavier Gaussian initialization, for MNIST training using a 3-states quantized activation for layer numbers near the depth scale $6\xi_{max} \simeq 37$. For each number of layers and initialization, we used a grid search to find best learning rate from the values $[0.25, 0.5, 1, 2, 4, 10] \times 10^{-3}$, with all other run parameters as described in the experimental part of section 5. We ran 25 seeds using that learning rate, and the plot describes the mean and standard error of the test accuracy, at every step. In all cases, our suggested modification outperforms Xavier initialization by a small margin. With 40 layers, the network depth exceeds the theoretical depth scale, and all trainings fail.

K Additional Proofs

K.1

Proof that fixed point slope for sign activation can only be optimal for $\sigma_b = 0$. We would like to prove the the optimal slope at the fixed point for sign activation can only be achieved when we take σ_b to zero. First, we will use the implicit function theorem to calculate $\frac{d\hat{C}^*}{d\sigma_b}$ (\hat{C} is the hidden states covariance, as described in appendix B), using the fixed point equation:

$$F(\hat{C}^*, \sigma_b) = \hat{C}^* - \frac{2}{\pi} \arcsin(C^*) = 0$$

when $C^* = \frac{\hat{C}^* \sigma_w^2 + \sigma_b^2}{\sigma_w^2 + \sigma_b^2}$, $Q^* = \sigma_w^2 + \sigma_b^2$:

$$\frac{\partial F}{\partial \hat{C}^*} = 1 - \chi$$

When we χ can be expressed using 11. Also:

$$\begin{aligned} \frac{\partial F}{\partial \sigma_b} &= -\frac{2}{\pi} \frac{1}{\sqrt{1-(C^*)^2}} \frac{\partial C^*}{\partial \sigma_b} = \\ &= -\frac{2}{\pi} \frac{1}{\sqrt{1-(C^*)^2}} \frac{2\sigma_b \sigma_w^2 (1-\hat{C}^*)}{(\sigma_w^2 + \sigma_b^2)^2} = -\chi \frac{2\sigma_b (1-\hat{C}^*)}{Q^*} \end{aligned}$$

and using the implicit function theorem:

$$\frac{d\hat{C}^*}{d\sigma_b} = -\frac{\frac{\partial F}{\partial \sigma_b}}{\frac{\partial F}{\partial \hat{C}^*}} = \frac{\chi}{1-\chi} \frac{2\sigma_b (1-\hat{C}^*)}{Q^*}$$

we can now use it to calculate:

$$\frac{d\chi}{d\sigma_b} = \frac{2\sigma_w^2}{\pi (\sigma_w^2 + \sigma_b^2) \sqrt{1-(C^*)^2}} \left[-\frac{2\sigma_b}{Q^*} + \frac{C^*}{1-(C^*)^2} \frac{dC}{d\sigma_b} \right]$$

while:

$$\begin{aligned} \frac{dC}{d\sigma_b} &= \frac{\sigma_w^2}{\sigma_w^2 + \sigma_b^2} \frac{dC^*}{d\sigma_b} + \frac{2\sigma_b}{\sigma_w^2 + \sigma_b^2} - \frac{C^* \sigma_w^2 + \sigma_b^2}{(\sigma_w^2 + \sigma_b^2)^2} 2\sigma_b = \\ &= \frac{1}{Q^*} \left(\sigma_w^2 \frac{dC^*}{d\sigma_b} + 2\sigma_b (1-C^*) \right) \end{aligned}$$

so:

$$\frac{d\chi}{d\sigma_b} = \frac{2\sigma_w^2}{\pi (Q^*)^2 \sqrt{1-(C^*)^2}} \left[+\frac{C^*}{1-(C^*)^2} \left(\sigma_w^2 \frac{dC^*}{d\sigma_b} + 2\sigma_b (1-C^*) \right) - 2\sigma_b \right] =$$

$$\begin{aligned}
\frac{d\chi}{d\sigma_b} &= \frac{2\sigma_w^2}{\pi(Q^*)^2 \sqrt{1-(C^*)^2}} \left[+\frac{C^*}{1-(C^*)^2} \left(\sigma_w^2 \frac{\chi 2\sigma_b}{1-\chi} (1-C^*) \right) + 2\sigma_b \frac{C^*}{1+(C^*)} - 2\sigma_b \right] = \\
&= \frac{2\sigma_w^2}{\pi(Q^*)^2 (1+C^*) \sqrt{1-(C^*)^2}} \left[\frac{C^*}{1-C^*} \sigma_w^2 \frac{\chi}{1-\chi} \frac{2\sigma_b (1-\widehat{C}^*)}{Q^*} - 2\sigma_b \right] = \\
&= \frac{4\sigma_w^2 \sigma_b}{\pi(Q^*)^2 (1+C^*) \sqrt{1-(C^*)^2}} \left[\frac{C^* Q^*}{(1-\widehat{C}^*)} \sigma_w^2 \frac{\chi}{1-\chi} \frac{(1-\widehat{C}^*)}{Q^*} - 1 \right] = \\
&= \frac{2\sigma_b \chi}{(Q^*)(1+C^*)} \left[\frac{\chi C^*}{1-\chi} - 1 \right]
\end{aligned}$$

we learn that $\text{sign}\left(\frac{d\chi}{d\sigma_b}\right)$ depends on $\frac{\chi C^*}{1-\chi} - 1$. if for some value of σ_b, σ_w , $\frac{\chi C^*}{1-\chi} > 1$, then, $\frac{\chi C^*}{1-\chi} - 1$ will remain positive when increasing σ_b , since $\frac{d\chi}{d\sigma_b} > 0$ and $\frac{dC^*}{d\sigma_b} > 0$ results $\frac{d}{d\sigma_b} \frac{\chi C^*}{1-\chi} > 0$. The optimal (highest) value of χ for the given value of σ_w will therefore be achieved in the limit $\sigma_b \rightarrow \infty$, and we can use the slope equation to calculate it:

$$\lim_{\sigma_b \rightarrow \infty} \chi = \lim_{\sigma_b \rightarrow \infty} \frac{2\sigma_w^2}{\pi \sqrt{(\sigma_w^2 + \sigma_b^2)^2 - (\widehat{C}^* \sigma_w^2 + \sigma_b^2)^2}} = 0$$

(for this we use the fact that $\widehat{C}^* > 0$ for $\sigma_b > 0$)

And this contradicts our assumption that this is the highest value of χ , so $\frac{d\chi}{d\sigma_b}$ must be negative for all values of σ_b, σ_w . □

K.2

Proof that stochastic rounding results smaller slope at the fixed point. We have shown that the covariance mapping function with stochastic rounding is $\widehat{\mathcal{M}}(\widehat{C}) = f\left(\frac{C_u}{B}\right)$, when we denote $C_u(\widehat{C}) = \frac{\widehat{C}\sigma_w^2 + \sigma_b^2}{\sigma_w^2 + \sigma_b^2}$, $C_u^* = C_u(\widehat{C}^*)$, and $f(x)$ is a convex function for $0 \leq x \leq 1$ and the variable $B \geq 1$ is increasing as the variance of the stochastic rounding increase, and $B = 1$ gives us the mapping for deterministic function. We will show that $\frac{d\chi^*}{dB} < 0$, when χ^* is the fixed point slope. Using the implicit function theorem as we did in proof K.1, for the function:

$$F(\widehat{C}^*, B) = \widehat{C}^* - \widehat{\mathcal{M}}(\widehat{C}^*) = 0$$

for $\frac{\partial F}{\partial \widehat{C}^*}$ we get:

$$\frac{\partial F}{\partial \widehat{C}^*} = 1 - \chi^* > 0$$

when we used the definition of χ^* as the fixed point slop. For $\frac{\partial F}{\partial B}$, we get

$$\frac{\partial F}{\partial B} = -f'\left(\frac{C_u}{B}\right) \cdot \frac{-C_u}{B^2} > 0$$

using the implicit function theorem:

$$\frac{d\widehat{C}^*}{dB} = -\frac{\frac{dF}{dB}}{\frac{dF}{d\widehat{C}^*}} < 0$$

and since $\frac{d\widehat{C}_u^*}{dC^*} = \frac{\sigma_w^2}{\sigma_w^2 + \sigma_b^2} > 0$ this also means that:

$$\frac{dC^*}{dB} < 0 \quad (41)$$

from eq. 30 we know that:

$$\chi^* = \frac{2\sigma_w^2}{\pi Q^* \sqrt{\left(1 - \left(\frac{C_u^*}{B}\right)^2\right)}}$$

we can immediately see that for $\bar{C} \equiv \frac{C_u^*}{B}$, we get $\frac{d\chi^*}{d\bar{C}} > 0$, and from eq. 41 we get that $\frac{d\bar{C}}{dB} = \frac{B \frac{dC^*}{dB} - C_u^*}{B^2} < 0$ so the chain rule gives us $\frac{d\chi^*}{dB} < 0$. \square

L Neural tangent kernel for quantized activations

We consider the dynamics of training for deep, wide neural networks. We argue that the error at an average test point will not improve during early stages of training if the signal propagation conditions do not obtain, and thus ensuring signal propagation should have a beneficial effect on generalization error.

L.1 NTK setup

We consider full-batch gradient descent with regression loss in a continuous time setting. Defining a fitting error $\zeta_i = f(x_i) - y_i$ ⁵, the loss function is given by

$$\varphi = \frac{1}{2N_d} \sum_{i=1}^{N_d} \zeta_i^2.$$

The weights evolve in time according to

$$\frac{\partial \theta_p}{\partial t} = -\frac{\partial \varphi}{\partial \theta_p} = -\frac{1}{N_d} \sum_{i=1}^{N_d} \frac{\partial f(x_i)}{\partial \theta_p} \zeta_i$$

for all weights θ_p . The evolution of the network function is then given by

$$\frac{\partial f(x_i)}{\partial t} = \sum_p \frac{\partial f(x_i)}{\partial \theta_p} \frac{\partial \theta_p}{\partial t} = -\frac{1}{N_d} \sum_p \frac{\partial f(x_i)}{\partial \theta_p} \frac{\partial f(x_j)}{\partial \theta_p} \zeta_j \equiv -\frac{1}{N_d} [\Theta \zeta]_i$$

where p indexes all the weights of the neural network and we have defined the Gram matrix $\Theta \in \mathbb{R}^{N_d \times N_d}$ by

$$\Theta(x_i, x_j) = \sum_p \frac{\partial f(x_i)}{\partial \theta_p} \frac{\partial f(x_j)}{\partial \theta_p}. \quad (42)$$

This matrix is referred to as the Neural Tangent Kernel (NTK) in [14]. When considering this object at the infinite width limit, it is convenient to adopt the following parametrization for a fully connected network $f: \mathbb{R}^{n_0} \rightarrow \mathbb{R}^{n_{L+1}}$:

$$\begin{aligned} \phi(\alpha^{(0)}(x)) &= x \\ \alpha^{(l)}(x) &= \frac{\sigma_w}{\sqrt{n_{l-1}}} W^{(l)} \phi(\alpha^{(l-1)}(x)) + \sigma_b b^{(l)}, \quad l = 1, \dots, L \\ f(x) &= \alpha^{(L+1)}(x) \end{aligned} \quad (43)$$

⁵This can be generalized to other loss functions [15].

for input $x \in \mathbb{R}^{n_0}$ and weight matrices $W^{(l)} \in \mathbb{R}^{n_l \times n_{l-1}}$. The weights are initialized using $W_{ij}^{(l)} \sim \mathcal{N}(0, 1)$, $b_i^{(l)} \sim \mathcal{N}(0, 1)$. The output of this NTK network is identical to that of a standard network, yet the gradients are rescaled such that Θ remains finite when taking the infinite width limit. For an appropriately chosen learning rate the dynamics of learning in the NTK network can be made identical to those of a standard network [15].

In [14], under some technical conditions, Θ was shown to be essentially constant during training at the sequential limit $\lim_{n_{L-1} \rightarrow \infty} \dots \lim_{n_2 \rightarrow \infty} \lim_{n_1 \rightarrow \infty}$. At this limit, adapting Theorem 1 of [14] to allowing arbitrary variances for the weights and biases, one obtains the following asymptotic form of Θ at the sequential infinite width limit:

$$\bar{\Theta}(x, x') = \sum_{l=1}^{L+1} \prod_{j=l+1}^{L+1} \Sigma^{(j)}(x, x') \Sigma^{(l)}(x, x') \quad (44)$$

where

$$\begin{aligned} \Sigma^{(1)}(x, x') &= \frac{\sigma_w^2}{n_0} x^T x' + \sigma_b^2 \\ \Sigma^{(l)}(x, x') &= \sigma_w^2 \mathbb{E}_{(u_1, u_2) \sim \mathcal{N}(0, \Sigma^{(l-1)}|_{x, x'})} \phi(u_1) \phi(u_2) + \sigma_b^2 \\ \Sigma^{(l)}|_{x, x'} &= \begin{pmatrix} \Sigma^{(l)}(x, x) & \Sigma^{(l)}(x, x') \\ \Sigma^{(l)}(x, x') & \Sigma^{(l)}(x', x') \end{pmatrix}. \end{aligned} \quad (45)$$

are the covariances of the pre-activations and

$$\Sigma^{(l)}(x, x') = \sigma_w^2 \mathbb{E}_{(u_1, u_2) \sim \mathcal{N}(0, \Sigma^{(l)}|_{x, x'})} \phi'(u_1) \phi'(u_2).$$

In [2] it was also shown that for finite width ReLU networks $\mathbb{E}\Theta = \bar{\Theta}$ and concentrates about its expectation with the fluctuations scaling inversely with layer width. It follows that when taking the layer widths to infinity in arbitrary order for ReLU networks one recovers $\bar{\Theta}$, and empirically Θ concentrates well around $\bar{\Theta}$ for other choices of nonlinearities [15]. We note that even when using the standard scaling 1, for very wide networks where the effect of individual weights will be negligible, even though the asymptotic form of the NTK at infinite width may be different, it will still change little in the initial phases of training.

L.2 Continuous activations

We write the NTK for a feed-forward network in the NTK parametrization 43, omitting the dependence on x of $f, \alpha^{(l)}$ to lighten notation

$$\begin{aligned} \frac{\partial f}{\partial W_{ij}^{(l)}} &= \frac{\sigma_w}{\sqrt{n_{l-1}}} \frac{\partial f}{\partial \alpha_i^{(l)}} \phi(\alpha_j^{(l-1)}) = \frac{\sigma_w}{\sqrt{n_{l-1}}} \frac{\partial f}{\partial \phi(\alpha_i^{(l)})} \frac{\partial \phi(\alpha_i^{(l)})}{\partial \alpha_i^{(l)}} \phi(\alpha_j^{(l-1)}) \\ &= \sum_{k=1}^{n_{l+1}} \frac{\sigma_w}{\sqrt{n_{l-1}}} \frac{\partial f}{\partial \alpha_k^{(l+1)}} \frac{\partial \alpha_k^{(l+1)}}{\partial \phi(\alpha_i^{(l)})} \frac{\partial \phi(\alpha_i^{(l)})}{\partial \alpha_i^{(l)}} \phi(\alpha_j^{(l-1)}) \\ &= \frac{\sigma_w}{\sqrt{n_{l-1}}} \sum_{k=1}^{n_{l+1}} \frac{\partial f}{\partial \alpha_k^{(l+1)}} \frac{\sigma_w}{\sqrt{n_l}} W_{ki}^{(l+1)} \frac{\partial \phi(\alpha_i^{(l)})}{\partial \alpha_i^{(l)}} \phi(\alpha_j^{(l-1)}) \end{aligned}$$

restoring the x dependence and defining a diagonal matrix $D^{(l)}(x) = \text{diag}(\frac{\sigma_w}{\sqrt{n_l}} \frac{\partial \phi(\alpha_i^{(l)}(x))}{\partial \alpha_i^{(l)}(x)})$ we have

$$\frac{\partial f(x)}{\partial W_{ij}^{(l)}} = \frac{\sigma_w}{\sqrt{n_{l-1}}} \left[\left(\frac{\partial f(x)}{\partial \alpha^{(l+1)}(x)} \right)^T W^{(l+1)} D^{(l)}(x) \right]_i \phi(\alpha_j^{(l-1)}(x))$$

we can repeat the process for the elements of $\frac{\partial f(x)}{\partial \alpha^{(l+1)}}$ finally obtaining

$$\frac{\partial f(x)}{\partial W_{ij}^{(l)}} = \frac{\sigma_w}{\sqrt{n_{l-1}}} \left[W^{(L+1)} D^{(L)}(x) W^{(L)} \dots W^{(l+1)} D^{(l)}(x) \right]_i \phi(\alpha_j^{(l-1)}(x)) \equiv \frac{\sigma_w}{\sqrt{n_{l-1}}} \widehat{\beta}_i^{(l)}(x) \widehat{\alpha}_j^{(l)}(x)$$

and we similarly obtain

$$\frac{\partial f(x)}{\partial b_i^{(l)}} = \sigma_b \widehat{\beta}_i^{(l)}(x).$$

The NTK thus takes the form

$$\begin{aligned} \Theta(x, x') &= \sum_{l, i_l} \frac{\partial f(x)}{\partial W_{i_l i_{l-1}}^{(l)}} \frac{\partial f(x')}{\partial W_{i_l i_{l-1}}^{(l)}} + \sum_{l, i_l} \frac{\partial f(x)}{\partial b_{i_l}^{(l)}} \frac{\partial f(x')}{\partial b_{i_l}^{(l)}} \\ &= \sigma_w^2 \sum_{l=1}^{L+1} \frac{1}{n_{l-1}} \left\langle \widehat{\beta}^{(l)}(x), \widehat{\beta}^{(l)}(x') \right\rangle \left\langle \widehat{\alpha}^{(l)}(x), \widehat{\alpha}^{(l)}(x') \right\rangle + \sigma_b^2 \left\langle \widehat{\beta}^{(l)}(x), \widehat{\beta}^{(l)}(x') \right\rangle \end{aligned}$$

According to [14, 2], this tends to 44 at the infinite width limit.

L.3 Quantized activations

We now consider dynamics in function space with quantized activations. Analyzing a single network in this fashion is hopeless since the network function is not a continuous function of the weights and so the dynamics will not be continuous. We can instead consider a stochastic rounding scheme where the post-activations are defined according to

$$\widehat{\alpha}_i^{(l)} = \text{sign}(\alpha_i^{(l)} - z_i^{(l)})$$

and $z_i^{(l)} \sim \text{Unif}([-1, 1])$. The connection between this setup and the straight-through estimator (STE) was first observed in [13]. We denote the set of all $z_i^{(l)}$ by $\{z\}$. Considering the dynamics of an ensemble average such that the loss function is given by

$$\varphi = \frac{1}{2N_d} \sum_{i=1}^{N_d} (\mathbb{E}_{\{z\}} f(x_i) - y_i)^2 = \frac{1}{2N_d} \sum_{i=1}^{N_d} \zeta_i^2$$

We have

$$\begin{aligned} \frac{\partial \mathbb{E}_{z_i^{(l)}} f}{\partial \alpha_i^{(l)}} &= \frac{\partial}{\partial \alpha_i^{(l)}} \left(p(\alpha_i^{(l)} - z_i^{(l)} > 0 | \alpha_i^{(l)}) f|_{\widehat{\alpha}_i^{(l)}=1} + (1 - p(\alpha_i^{(l)} - z_i^{(l)} > 0 | \alpha_i^{(l)})) f|_{\widehat{\alpha}_i^{(l)}=-1} \right) \\ &= \frac{\partial p(\alpha_i^{(l)} - z_i^{(l)} > 0 | \alpha_i^{(l)})}{\partial \alpha_i^{(l)}} \left(f|_{\widehat{\alpha}_i^{(l)}=1} - f|_{\widehat{\alpha}_i^{(l)}=-1} \right) = \frac{1}{2} \mathbb{1}_{|\alpha_i^{(l)}| \leq 1} \left(f|_{\widehat{\alpha}_i^{(l)}=1} - f|_{\widehat{\alpha}_i^{(l)}=-1} \right). \end{aligned}$$

If we now consider any smooth extension of γ of $\widehat{\alpha}_i^{(l)}$ such that $[-1, 1] \subseteq \text{Im}(\gamma)$ and denote by \tilde{f} a copy of f where we replace $\widehat{\alpha}_i^{(l)}$ by γ . We then have

$$f|_{\widehat{\alpha}_i^{(l)}=1} - f|_{\widehat{\alpha}_i^{(l)}=-1} = \tilde{f}|_{\gamma=1} - \tilde{f}|_{\gamma=-1} = \frac{\partial \tilde{f}}{\partial \gamma} \Big|_{\gamma=0} + \mathcal{O} \left(\frac{\partial^3 \tilde{f}}{\partial \gamma^3} \Big|_{\gamma=0} \right) = \frac{\partial \tilde{f}}{\partial \gamma} \Big|_{\gamma=0} + \mathcal{O} \left(\frac{\partial^3 \tilde{f}}{\partial \gamma^3} \Big|_{\gamma=0} \right)$$

$$= \frac{\partial \tilde{f}}{\partial \gamma} \Big|_{\gamma=\pm 1} + \mathcal{O} \left(\frac{\partial^2 \tilde{f}}{\partial \gamma^2} \Big|_{\gamma=0} \right) = \frac{\partial f}{\partial \hat{\alpha}_i^{(l)}} \Big|_{\hat{\alpha}_i^{(l)}=\pm 1} + \mathcal{O} \left(\frac{\partial^2 \tilde{f}}{\partial \gamma^2} \Big|_{\gamma=0} \right) = \frac{\partial \mathbb{E}_{z_i^{(l)}} f}{\partial \hat{\alpha}_i^{(l)}} + \mathcal{O} \left(\frac{\partial^2 \tilde{f}}{\partial \gamma^2} \Big|_{\gamma=0} \right).$$

If we neglect these higher order terms (which should be small since the influence of a single neuron on the output is generally small, and should vanish at the infinite width limit) and note that the above approximation holds if we condition on $\{z\} \setminus \{z_i^{(l)}\}$, we obtain

$$\frac{\partial \mathbb{E}_{\{z\}} f}{\partial \alpha_i^{(l)}} \approx \mathbb{1}_{|\alpha_i^{(l)}| \leq 1} \frac{\partial \mathbb{E}_{\{z\}} f}{\partial \hat{\alpha}_i^{(l)}}. \quad (46)$$

We can now repeat the calculation of the NTK using eq. 46, obtaining

$$\begin{aligned} \frac{\partial \mathbb{E}_{\{z\}} f}{\partial W_{ij}^{(l)}} &= \frac{\sigma_w}{\sqrt{n_{l-1}}} \frac{\partial \mathbb{E}_{\{z\}} f}{\partial \alpha_i^{(l)}} \phi(\alpha_j^{(l-1)}) \approx \frac{\sigma_w}{\sqrt{n_{l-1}}} \frac{\partial f}{\partial \phi(\alpha_i^{(l)})} \mathbb{1}_{|\alpha_i^{(l)}| \leq 1} \phi(\alpha_j^{(l-1)}) \\ &= \frac{\sigma_w}{\sqrt{n_{l-1}}} \sum_{k=1}^{n_{l+1}} \frac{\partial f}{\partial \alpha_k^{(l+1)}} \frac{\sigma_w}{\sqrt{n_l}} W_{ki}^{(l+1)} \mathbb{1}_{|\alpha_i^{(l)}| \leq 1} \phi(\alpha_j^{(l-1)}). \end{aligned}$$

Defining $D_{\text{STE}}^{(l)}(x) = \text{diag}(\frac{\sigma_w}{\sqrt{n_l}} \mathbb{1}_{|\alpha_i^{(l)}| \leq 1})$ and applying eq. 46 repeatedly at each layer up until $L+1$ gives

$$\begin{aligned} \frac{\partial f(x)}{\partial W_{ij}^{(l)}} &\approx \frac{\sigma_w}{\sqrt{n_{l-1}}} \left[W^{(L+1)} D_{\text{STE}}^{(L)}(x) W^{(L)} \dots W^{(l+1)} D_{\text{STE}}^{(l)}(x) \right]_i \phi(\alpha_j^{(l-1)}(x)) \equiv \frac{\sigma_w}{\sqrt{n_{l-1}}} \hat{\beta}_{\text{STE},i}^{(l)}(x) \hat{\alpha}_j^{(l)}(x) \\ \frac{\partial f(x)}{\partial b_i^{(l)}} &\approx \sigma_b \hat{\beta}_{\text{STE},i}^{(l)}(x). \end{aligned}$$

and thus applying 42 gives

$$\frac{\partial \mathbb{E}_{\{z\}} f(x)}{\partial t} \approx -\frac{1}{N_d} \sum_i \Theta_{\text{STE}}(x, x_i) \zeta_i$$

where

$$\Theta_{\text{STE}}(x, x') = \sigma_w^2 \sum_{l=1}^{L+1} \frac{1}{n_{l-1}} \left\langle \hat{\beta}_{\text{STE}}^{(l)}(x), \hat{\beta}_{\text{STE}}^{(l)}(x') \right\rangle \left\langle \hat{\alpha}^{(l)}(x), \hat{\alpha}^{(l)}(x') \right\rangle + \sigma_b^2 \left\langle \hat{\beta}_{\text{STE}}^{(l)}(x), \hat{\beta}_{\text{STE}}^{(l)}(x') \right\rangle.$$

A trivial generalization of the calculation of the asymptotic form of $\Theta(x, x')$ at the infinite width limit in [14] shows that at this limit $\Theta_{\text{STE}}(x, x')$ tends to

$$\bar{\Theta}_{\text{STE}}(x, x') = \sum_{l=1}^{L+1} \prod_{j=l+1}^{L+1} \Sigma'_{\text{STE}}(j)(x, x') \Sigma^{(l)}(x, x') \quad (47)$$

where $\Sigma^{(l)}(x, x')$ is defined in eq. 45,

$$\Sigma'_{\text{STE}}(l)(x, x') = \sigma_w^2 \mathbb{E}_{(u_1, u_2) \sim \mathcal{N}(0, \Sigma^{(l)}|_{x, x'})} \phi'_{\text{STE}}(u_1) \phi'_{\text{STE}}(u_2).$$

and we define the hard-tanh function,

$$\phi_{\text{STE}}(x) = \begin{cases} 1 & 1 \leq x \\ x & -1 < x < 1 \\ -1 & x \leq -1 \end{cases} \quad (48)$$

for which $\phi'_{\text{STE}}(y) = \mathbb{1}_{|y| \leq 1}$. The form of $\bar{\Theta}_{\text{STE}}(x, x')$ is thus obtained by replacing the sign activation with eq. 48 but only during the backwards pass (and not during the forward pass), in line with the motivation of the STE in [13]. We note that the dynamics of this ensemble average correspond to those of the update scheme in eq. 19 with $\rho = 1$. Other choices will introduce a dependence on ρ in $\bar{\Theta}_{\text{STE}}(x, x')$ but will not change the fact that it can be expressed as a function of the covariances of the inputs in eq. 45.

L.4 Asymptotic NTK and generalization

We now consider a very deep network such that the covariance map approaches its fixed point

$$\Sigma^*|_{x, x'} = Q^* \begin{pmatrix} 1 & C^* \\ C^{* *} & 1 \end{pmatrix}.$$

$\Theta^{(l)}(x, x')$ for very deep networks will approach a matrix of the form

$$\lim_{L \rightarrow \infty} \frac{1}{L+1} \Theta^{(L+1)}(x, x') = \Theta^*(x, x') = \alpha \delta(x, x') + \beta(1 - \delta(x, x')) \quad (49)$$

for some constants α, β and $\delta(x, x')$ is a Kronecker delta.

To understand the generalization properties of such a network, we can consider the evolution of the error at some test point z that is not part of the training set. It will be given by

$$\frac{\partial \zeta(z)}{\partial t} = -\frac{L}{N_d} \sum_{i=1}^{N_d} \Theta^*(z, x_i) \zeta(x_i) = -\frac{\beta L}{N_d} \sum_{i=1}^{N_d} \zeta(x_i)$$

which at initialization is independent of our choice of z . Since it is also independent of the true label of z this will mean that the generalization error will typically not decrease⁶.

We conclude that for networks deep enough that the covariance map converges, in the initial phase of training before Θ changes considerably there will be no improvement in the generalization error at a typical test point. Conversely, this suggests that satisfying the signal propagation condition $\chi = 1$ will facilitate generalization. Presumably, if convergence to the fixed point is slow, instead of the form in eq. 49, Θ will exhibit some finite scale of decay from its value on the diagonal as a function of the distance between the inputs. This will enable points in the training set near z that share the same label, and where the error has the same sign as $\zeta(z)$, to influence $\frac{\partial \zeta(z)}{\partial t}$ thus reducing the error at z . This argument is independent of the value of β , and provides further motivation for the study of critical initialization schemes that exhibit slow convergence to the fixed point [25]. Such initialization schemes have also been motivated in the past by concerns of trainability (i.e. ensuring stable signal propagation from the inputs to the hidden states of a deep network, and preventing vanishing/exploding gradients). This phenomenon could perhaps be the basis for the improvements in generalization observed when using critical initialization schemes, which have hitherto been unexplained.

To explore whether rapid convergence of the covariance map is correlated with a lack of structure in the NTK, we define a coarse metric for non-trivial structure in the off-diagonal terms of the NTK that should facilitate generalization. Given a row of the NTK $\Theta_i = \Theta(x_i, \cdot) \in \mathbb{R}^{N_d}$, we define our signal

⁶Aside from some trivial cases such as learning a constant function.

to be the sum of off-diagonal terms in this row that share a label with x_i :

$$S_i = \sum_{\substack{j \neq i \\ y_j = y_i}} \Theta(x_i, x_j)$$

while the corresponding noise measure is simply

$$N_i = \|\Theta_i\|_1 - S_i.$$

The idea behind this metric is that the fitting error at some $\zeta(x_j)$ with $y_i = y_j$ will be closer on average to $\zeta(x_i)$ than $\zeta(x_j)$ such that $y_j \neq y_i$. If x_i is not part of the training set, $\frac{\partial \zeta(x_i)}{\partial t} = -\frac{1}{N_d} \sum_{j=1, j \neq i}^{N_d} \Theta(x_i, x_j) \zeta(x_j)$. Thus if the elements of Θ with the same label as x_i are large and positive there will be a large magnitude contribution to $\frac{\partial \zeta(x_i)}{\partial t}$ that has the opposite sign as $\zeta(x_i)$ and thus $\zeta(x_i)$ will decrease quickly over time. The noise in this case is the size of the other entries. Generalization error should thus improve if the signal-to-noise ratio

$$\text{SNR} = \frac{1}{N_d} \sum_i \frac{S_i}{N_i} \quad (50)$$

is large and

$$S = \frac{1}{N_d} \sum_i S_i \quad (51)$$

is large as well. The latter condition is important since in the case of networks with small weight variance SNR may be large but S itself vanishes and so will any change in the generalization error. For both networks with tanh and quantized activation we observe that the regime where SNR and S are both large corresponds to the one where the signal propagation time scale in eq. 7 is large as well, as shown in Figure 11.

In this experiment, the network architecture is given by 1 with $L = 30$ and all hidden layers of width 300. Note that for a finite width network with constant layer widths the difference between the NTK and that of a network given by 43 will be a constant factor. The quantities in the plot are averaged over 450 MNIST data points for the tanh network and 200 images for the quantized network, and 5 different initializations. The NTK for the network with quantized activations is calculated by replacing the terms in the backwards pass with the STE equivalents, as in 47.

L.5 Change of asymptotic NTK during training

We have argued above that based on the structure of the NTK at initialization for networks where the covariance map has converged, we expect no initial improvement in the generalization error. At later times, if we assume that the Taylor expansion of Θ_t^* exists

$$\Theta_t^*(z, x') = \sum_{k=0}^{\infty} \frac{t^k}{k!} \frac{\partial^k \Theta_0^*(z, x')}{\partial t^k}$$

we can see directly that $\Theta_t^*(z, x')$ will be independent of z as well, since the summands in the RHS are. This argument thus extends to later times asymptotically at the infinite width limit, or for finite width until such time as deviations from the asymptotic form of the NTK influence the dynamics.

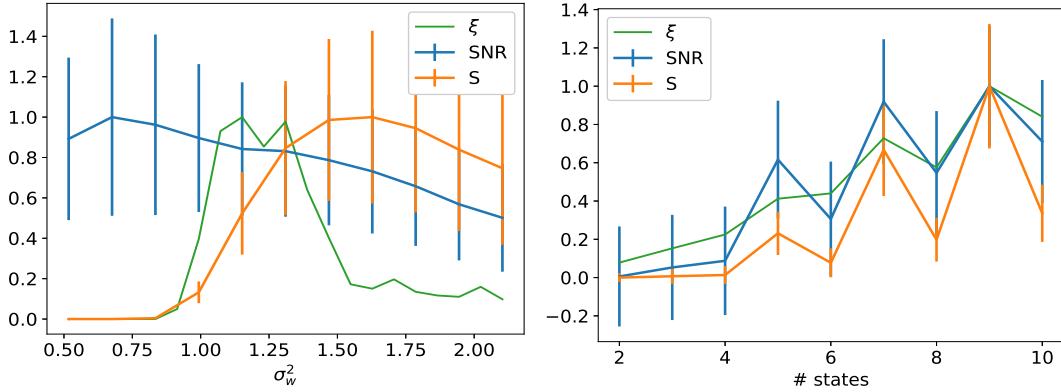


Figure 11: Off-diagonal structure in the NTK is correlated with signal propagation. The signal (eq. 51) that is expected to improve generalization, the signal-to-noise ratio (eq. 50) and the signal propagation time scale (eq. 7) are plotted for different architectures. All quantities are normalized by the maximal value in the range of parameters shown. *Left:* For networks with tanh activations with different weight variance σ_w^2 , the time scale ξ behaves non-monotonically. The SNR decreases monotonically, while the signal S spikes around the same value of σ_w^2 where signal propagation is best achieved. Thus the point that maximizes both SNR and S is close to the one where signal propagation is also maximal. *Right:* For networks with quantized activations, as the quantization level increases so does the SNR and the signal itself. We also observe the same non-monotonic behaviour based on the parity of the number of states in all three.